Journal of Medicinal Chemistry

Article

Discovery of a novel and selective Indoleamine 2,3-dioxygenase (IDO-1) inhibitor 3-(5-fluoro-1*H*-indol-3-yl)pyrrolidine-2,5-dione (EOS200271/ PF-06840003) and its characterization as a potential clinical candidate

Stefano Crosignani, Patrick Bingham, Pauline Bottemanne, Hélène Cannelle, Sandra Cauwenberghs, Marie Cordonnier, Deepak Dalvie, Frederik Deroose, Jun Li Feng, Bruno Gomes, Samantha Greasley, Stephen E. Kaiser, Manfred Kraus, Michel Négrerie, Karen A. Maegley, Nichol Miller, Brion W. Murray, Manfred Schneider, James Solowiej, Albert E Stewart, Joseph Tumang, Vince R Torti, Benoit Van den Eynde, and Martin Wythes

J. Med. Chem., **Just Accepted Manuscript** • DOI: 10.1021/acs.jmedchem.7b00974 • Publication Date (Web): 07 Nov 2017

ACS Publications

Journal of Medicinal Chemistry is published by the American Chemical Society. 1155 Sixteenth Street N.W., Washington, DC 20036

Discovery of a novel and selective Indoleamine 2,3-dioxygenase (IDO-1) inhibitor 3-(5-fluoro-1*H*-indol-3-yl)pyrrolidine-2,5-dione (EOS200271/PF-06840003) and its characterization as a potential clinical candidate

Stefano Crosignani[*,§], *Patrick Bingham*[†], *Pauline Bottemanne*[§], *Hélène Cannelle*[§], *Sandra Cauwenberghs*[§], *Marie Cordonnier*[§], *Deepak Dalvie*[†], *Frederik Deroose*[¥], *Jun Li Feng*[†], *Bruno Gomes*[§], *Samantha Greasley*[†], *Stephen E Kaiser*[†], *Manfred Kraus*[†], *Michel Négrerie*[ǀ], *Karen Maegley*[†], *Nichol Miller*[†], *Brion W Murray*[†], *Manfred Schneider*[§], *James Soloweij*[†], *Albert E Stewart*[†], *Joseph Tumang*[†], *Vince R Torti*[†], *Benoit Van Den Eynde*[ǀ] , *Martin Wythes*[†]*

[§] iTeos Therapeutics, Rue des Frères Wright 29, 6041 Gosselies, Belgium

[†] Pfizer Global Research and Development, La Jolla Laboratories, 10770 Science Center Dr., San Diego, CA 92121, USA

[ǀ] Ludwig Institute for Cancer Research, Université Catholique de Louvain, 74 Avenue Hippocrate, 1200 Brussels, Belgium

[¥] Asclepia Outsourcing Solutions, Damvalleistraat 49, Destelbergen, 9070, Belgium

[I] Ecole Polytechnique, Unité Inserm 1182 UMR 7645, Route de Saclay, Palaiseau, 91128, France

KEYWORDS Indoleamine-2,3-dioxygenase 1; Cancer immunotherapy.

ABSTRACT. Tumors use tryptophan-catabolizing enzymes such as Indoleamine 2,3-dioxygenase (IDO-1) to induce an immunosuppressive environment. IDO-1 is induced in response to inflammatory stimuli and promotes immune tolerance through effector T-cell anergy and enhanced Treg function. As such, IDO-1 is a nexus for the induction of key immunosuppressive mechanism and represents an important immunotherapeutic target in oncology. Starting from HTS hit **5**, IDO-1 inhibitor **6** (EOS200271/PF-06840003) has been developed. SAR around **6** is described and rationalized using the X-ray crystal structure of **6** bound to human IDO-1, which shows that **6**, differently from most of the IDO-1 inhibitors described so far, does not bind to the heme iron atom and has a novel binding mode. Clinical candidate **6** shows good potency in an IDO-1 human whole blood assay, and also shows a very favorable ADME profile leading to favorable predicted human pharmacokinetic properties, including a predicted half-life of 16-19 hours.

Introduction

Immune checkpoints blockade, as a breakthrough in cancer therapy with anti-PDL1 (Programmed death-ligand 1), anti-PD1 (Programmed cell death protein 1), and anti-CTLA4 (cytotoxic T-lymphocyte-associated protein 4), has demonstrated impressive therapeutic effects in multiple clinical trials.[1] However, only a small minority of patients respond to such therapies. Therefore, there is a need to identify other tumor immunosuppressive and resistance mechanisms.

Indoleamine 2,3-dioxygenase (IDO-1) is a heme-containing dioxygenase that contributes to metabolic immune regulation by catalyzing oxidative catabolism of the essential amino-acid tryptophan to *N*-formyl kynurenine. After this first and rate-limiting step of tryptophan catabolism, *N*-formyl kynurenine is subsequently converted to kynurenine and other immunologically active metabolites via the kynurenine pathway. IDO-1 modifies immune response by producing biologically active kynurenine-pathway metabolites, natural ligands for the aryl hydrocarbon receptor (AhR), and by depleting tryptophan to trigger amino-acid sensing signal transduction pathways.[2,3] Given the IDO-1 enzymatic activity-mediated suppression of T-cell responses[4] and the correlation between IDO-1 expression and poor prognosis and chemoresistance in several cancer indications,[5-7] IDO-1 is a target of interest for cancer immunotherapy. Indeed, potential IDO-1-inhibiting drugs for use in human cancers are now the focus of research and development efforts.[8-9]

At the time this project was started, only one IDO-1 inhibitor was in clinical trials, INCB24360.[10] Considering the high attractiveness of the target, as well as the limitations of this compound, which despite its good potency still requires a relatively high dose to reach full inhibition of the target, and which has a relatively short half-life in man and requires BID administration, it was important to discover novel IDO-1 inhibitors, with the potential to become clinically-relevant therapeutics for oncology immunotherapy.

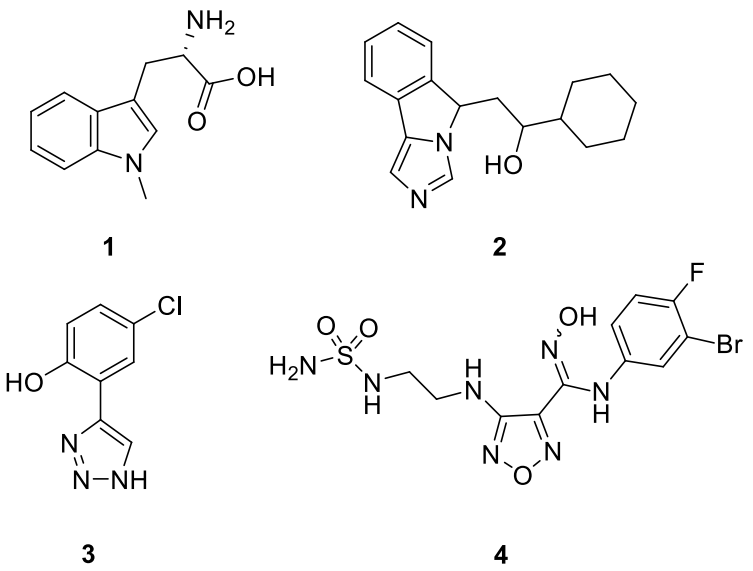

Figure 1. Some inhibitors of hIDO-1.

Results and Discussion

A library of 178000 diverse compounds was screened using a modification of the published hIDO-1 enzymatic assay (based on detection of *N*-formyl kynurenine by measuring absorbance at 320 nm), adapted for 384-well plate format.[11] Among the confirmed hits, the most promising for subsequent optimization was compound **5**. When tested on the *p*-dimethylamino benzaldehyde assay (based on detection of kynurenine after formation of an adduct with *p*-dimethylamino benzaldehyde, PDMAB),[12] this compound showed a moderate potency on hIDO-1 in the enzymatic assay (IC_{50} 3.0 μM) but no activity on tryptophan 2,3-dioxygenase (hTDO-2, up to 50 μM). Given its extremely low molecular weight, the compound had a good ligand efficiency (LE) of 0.47 highlighting the high efficiency of interaction of the compound with hIDO-1. Other indole-containing compounds have been reported as hIDO-1 inhibitors, but all with reported K_is of >10 μM.[13-20]

Of the two enantiomers of **5**, only one showed appreciable activity on hIDO-1 in the enzymatic assay (**5a**, IC_{50} 1.8 μM), whereas the other enantiomer (**5b**) had only marginal activity on hIDO-1 (IC_{50} 83 μM). The active enantiomer **5a** was further profiled to assess its suitability as a starting point for further optimization.

Of particular interest, the compound displayed a very attractive ADME profile (Table 1): a very moderate protein binding, excellent stability in human and mouse microsomes and excellent permeability in a Caco-2 assay (with no active efflux). Additionally, no significant cytochrome P450 (CYP) inhibition was observed on five isoforms (IC_{50}s > 50 μM on 1A2, 2C19, 2C9, 2D6 and 3A4). *In vivo*, **5a** also displayed an excellent profile in mice, with moderate Clearance (15.6 mL/min/kg, 17% Q_H), medium volume of distribution and good oral bioavailability (63% and 65% respectively at 5 and 30 mg/kg, using a simple suspension administration).

Overall, despite the moderate potency, **5a** was considered a good starting point for further optimization.

Table 1. Profile of hit **5a**

hIDO-1 IC_{50} (μM)	1.8
PPB (h/m, Fu)	43% / 55%
Microsomal Clint (h/m; μL/min/μg)	<10 / <10
Caco-2 Papp (10^{-6} cm/s)	28 (efflux ratio 0.77)
CYP450 IC_{50} (1A2, 2C9, 2C19, 2D6, 3A4; μM)	>10
Mouse PK Cl (mL/min/kg)	15.6
Mouse PK Vss (L/kg)	1.2
Mouse PK $t_{1/2}$ (h)	0.97

Mouse PK Fz (5 and 30 mg/kg)	63% / 65%

Chemistry. Generally, 3-(3-indolyl)-succinimides could be easily prepared by heating the corresponding indoles (commercially available or prepared according to published procedures) with maleimide in acetic acid, either at reflux for several hours, or at higher temperatures in a microwave apparatus (Scheme 1). For scaling-up, the reaction conditions for this coupling in acetic acid were found to generate a significant number of by-products, so a milder alternative was sought. A number of Lewis Acids were tested as catalysts for the reaction, and zinc chloride in acetonitrile, at 85 °C was found to give excellent conversions and to give a product easy to purify by a simple recrystallization, at least for the preparation of compound **6**. Nitriles **9** and **17** were obtained from the corresponding bromides **8** and **16**, by copper-catalyzed cyanation (Scheme 1).

Scheme 1. Synthesis of Indole Derivatives 1-24.[a]

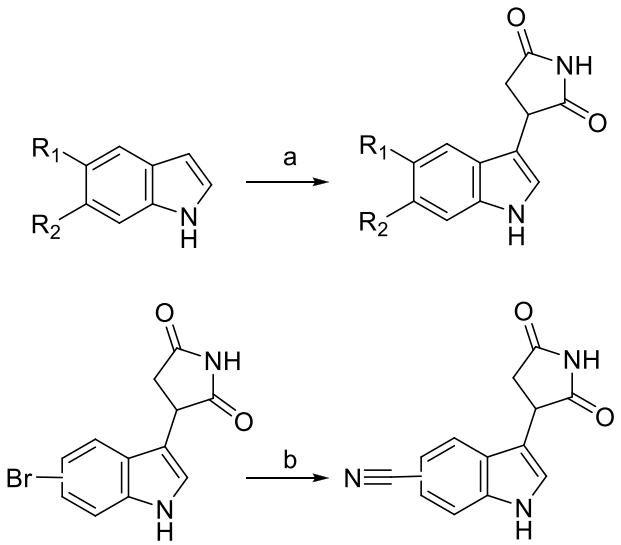

[a]Reagents and conditions: (a) Maleimide, acetic acid, 170 °C (microwave irradiation), 2h. (b) CuCN, NMP, 200 °C (microwave irradiation) 1.5 h

3-(1-Naphthyl)-succinimide **25** was prepared starting from 1-napthyl-boronic acid, by $[RhOH(cod)]_2$-catalyzed coupling with maleimide (Scheme 2). Substituted 3-(1-Naphthyl)-succinimides were prepared from the corresponding 1-nephthalene-amines, via the respective diazo salts and then succinic acids (Scheme 2).

Scheme 2. Synthesis of Naphthalene Derivatives **25**-**29**.[a]

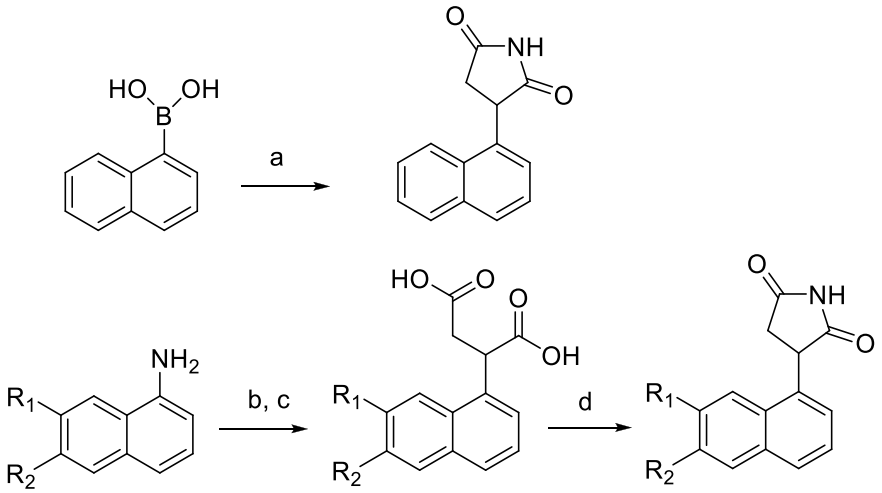

[a]Reagents and conditions: (a) Maleimide, $[RhOH(cod)]_2$, Et_3N, dioxane, 50 °C, 2.5 h; (b) HBF_4, $NaNO_2$, H_2O, 0 °C-RT, 1h; (c) Maleic anhydride, $TiCl_3$, water/acetone; (d) urea, 180 °C, 1h.

Biological activity. Systematic SAR was performed on both halves of the molecule (Table 2). It soon became apparent that the succinimide could not be modified without very significant drops in activity (list of molecules with full biological data in Supporting Information). Removal of either or both of the carbonyl groups to give either the regioisomeric pyrrolidinones or the corresponding pyrrolidine, or ring expansion to the corresponding glutarimide (either regioisomer) all gave compounds with $IC_{50} > 30$ μM. Similarly, substitution with a methyl group on either the succinimide nitrogen or on either of the two succinimide aliphatic carbon atoms (with any stereochemistry) resulted in loss of more than an order of magnitude of activity. Also,

replacing the succinimide CH_2 group with either a nitrogen or oxygen atom resulted in compounds with $IC_{50} > 50$ μM. Finally, inserting a CH_2 linker between the succinimide and indole groups also resulted in loss of activity.

Table 2. SAR of Indolyl and Naphthyl Succinimides

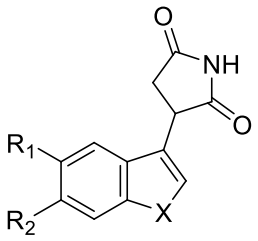

Compound	X	R1	R2	IC_{50} hIDO-1 (μM)[a]
5	NH	H	H	3.0
5a[b]	NH	H	H	1.8
5b[c]	NH	H	H	83
6	NH	F	H	0.15
6a[b]	NH	F	H	0.12
6b[c]	NH	F	H	54
7	NH	Cl	H	0.83
7a[b]	NH	Cl	H	2.2
7b[c]	NH	Cl	H	>50
8	NH	Br	H	0.37
9	NH	CN	H	1.2
10	NH	OMe	H	53
11	NH	Me	H	53
12	NH	CF_3	H	9.7

13	NH	H	F	3.4
14	NH	H	Cl	2.1
15	NH	H	Br	0.42
16	NH	H	CN	1.7
17	NH	H	OMe	>50
18	NH	H	Me	54
19	NH	F	F	1.8
20	NH	F	Cl	0.49
20a[b]	NH	F	Cl	0.58
20b[c]	NH	F	Cl	>50
21	NH	F	Br	0.29
21a[b]	NH	F	Br	0.62
21b[c]	NH	F	Br	8.0
22	NH	F	Me	46
23	CH=CH	H	H	18
24	CH=CH	F	H	4.6
25	CH=CH	H	F	1.7
26	CH=CH	Cl	H	>50
27	CH=CH	H	Cl	>50

[a] average of n≥2 independent experiments. [b] First enantiomer (by elution order in chiral HPLC). [c] Second enantiomer (by elution order in chiral HPLC).

Exploration of the indole group also quickly showed that some parts of the molecule were not free for substitution: methylation of the indole NH or of the C2 resulted in significant drop in activity, whereas substitution in positions C4 and C7 with either methyl, chlorine or methoxy

also gave compounds with IC_{50}s > 50 μM (full list of compounds with biological data in Supporting Information). On the other hand, substitution on positions C5 and C6 of the indole turned out to be more tolerated, and in some cases beneficial. In position 5, a clear preference was identified for halogens, with increase in activity for the fluoro (**6**, IC_{50} 0.15 μM), chloro (**7**, IC_{50} 0.83 μM) and bromo (**8**, IC_{50} 0.37 μM) substitutions, whereas substitution with methyl (**11**, IC_{50} 53 μM), methoxy (**10**, IC_{50} 53 μM) and CF_3 (**12**, IC_{50} 9.7 μM) groups led to significant loss of activity. In position 6, substitution with halogen was neutral for potency (F, **13**, IC_{50} 3.4 μM); Cl, **14**, IC_{50} 2.1 μM) or advantageous (Br, **15**, IC_{50} 0.42 μM), whereas other substitutions led to loss of potency, with the exception of the nitrile substituent (**16**, IC_{50} 1.7 μM).

Having identified **6** as the most potent mono-substituted compound, we tried a small number of doubly-substituted compounds based on this scaffold: as expected, adding a methyl group in position 6 (**22**, IC_{50} 46 μM) led to a significant drop in activity, but unfortunately adding either a fluorine (**19**, IC_{50} 1.8 μM), chlorine (**20**, IC_{50} 0.49 μM) or bromine (**21**, IC_{50} 0.29 μM) in position 6 did not yield any improvement in potency compared to **6**.

Finally, several replacements of the indole core with alternative heterocycles were attempted. Replacement with either indazole, benzimidazole, all four regioisomeric azaindoles, different isoquinoline and quinoline regioisomers, different indole regioisomers as well as substituted benzofurans and benzothiophenes were all found to be significantly less active (IC_{50} > 20 μM, full list of compounds with biological data in Supporting Information). The only replacement which maintained a significant potency on the target was found to be the 1-napthalene compound **23** (IC_{50} 18 μM). It was thus decided to explore if appropriate substitution with halogens might yield potent compounds. Unfortunately, the most potent compound in this sub-series was **24**,

which was still significantly less potent than **6** (IC_{50} 4.6 μM), while having significantly higher cLogP, and was thus not further pursued.

Compound **6** was separated into its pure enantiomers, **6** and **6b**. As observed for **5**, only one of the two enantiomers **6a** was responsible for the inhibition of IDO-1 in the enzymatic assay. The absolute configuration of the active enantiomer of **6** was determined by X-ray crystallography and found to be (R).

Subsequent to the discovery of **6a** further structural insights to its IDO-1 inhibition binding mode were sought, by X-ray and spectroscopic methods. IDO-1 has an active site heme cofactor which enables mechanistic characterization of inhibitor binding interactions. Heme is a porphyrin ring with an iron at its center which absorbs light in UV-vis spectrum maximally at a wavelength around 400 nm depending on the oxidation and coordination states of its iron – the Soret band.[22] Inhibitors that coordinate the heme iron will shift the Soret band λ_{max}. Inhibitors that do not directly coordinate the iron will only modulate the Soret band because the heme is highly-sensitive to changes in the polarity of its surroundings.[23] The observed Soret bands for the ferrous IDO-1 (λ_{max} 427 nm) and ferric IDO-1 (λ_{max} 405 nm) are in-line with values previously reported (Fe^{2+} form, 429; Fe^{3+} form 404 nm).[24] The IDO-1 inhibitors did not shift the Soret λ_{max} for either ferric or ferrous forms of IDO-1 which is not consistent with direct binding to the heme iron (**Figure 2**). The binding affinity of the IDO-1 inhibitors was determined by measuring the decrease in the Soret band absorbance. **6a** is shown to bind weakly to both the ferric and ferrous forms of IDO-1 in the presence of oxygen with apparent binding constants of 9 and 6 μM, respectively. Under conditions where the oxygen content is depleted, **6a** binds to the ferric form of IDO-1 with an apparent binding constant of 0.16 μM. This value is in-line with the IC_{50} value

determined kinetically and suggests that the ferric form, without oxygen bound at the heme, is the form of the enzyme that the inhibitor binds to during catalysis. Further analysis of the ferric form with depleted oxygen and added tryptophan showed that the affinity (K_d^{app} 0.15 μM) is similar to the value in the absence of tryptophan (**Table 3**). Since tryptophan does not bind this form of the enzyme tightly, **6a** is unlikely to be competitive with tryptophan. These findings are consistent with **6a** being a tryptophan non-competitive, non-heme binding IDO-1 inhibitor. Similar results were shown for the racemic compound, **6** indicating that the behavior of the racemic mixture and the pure enantiomer are comparable.

Table 3. Biochemical affinity analysis for different forms of IDO-1. Inhibition was determined by a decrease of the Soret band intensity (ferrous form λmax = 427 nm, ferric form λmax = 405 nm). Data are represented as geometric mean in μM, plus 95% confidence interval in parentheses determined from two independent experiments. Kd^{app} ferrous are derived from titrating the inhibitors into the ferrous form of IDO-1. Kd^{app} ferric is derived from titrating the inhibitors into the ferric form of IDO-1 without measures to remove oxygen. Kd^{app} ferric (depleted O2) is derived from titrating the inhibitors into the ferric form of IDO-1 following oxygen depletion. Kd^{app} ferric (depleted O_2, +Trp) is derived from titrating the inhibitors into the ferric form of IDO-1 in the presence of tryptophan following oxygen depletion. Kd^{app} is the apparent dissociation constant. NT = not tested.

	IDO-1 inhibitor binding to different forms of hIDO1 (μM)			
IDO-1 Inhibitor	K_d^{app} Ferrous	K_d^{app} Ferric	K_d^{app} Ferric (depleted O_2)	K_d^{app} Ferric (depleted O_2, +Trp)
6	14 (12-16)	22.3 (22.1-22.6)	0.32 (0.27-0.38)	NT
6a	6 (3-12)	7 (5-11)	0.16 (0.13-0.19)	0.15 (0.12-0.19)

Figure 2, panel A. Evaluation of **6**. (A) Ferrous hIDO1. (B) Ferric hIDO1 in the presence of oxygen. (C) Ferric hIDO1 after oxygen depletion (D) Ferric hIDO1 with tryptophan after oxygen depletion.

Figure 2, panel A. Ferrous hIDO1

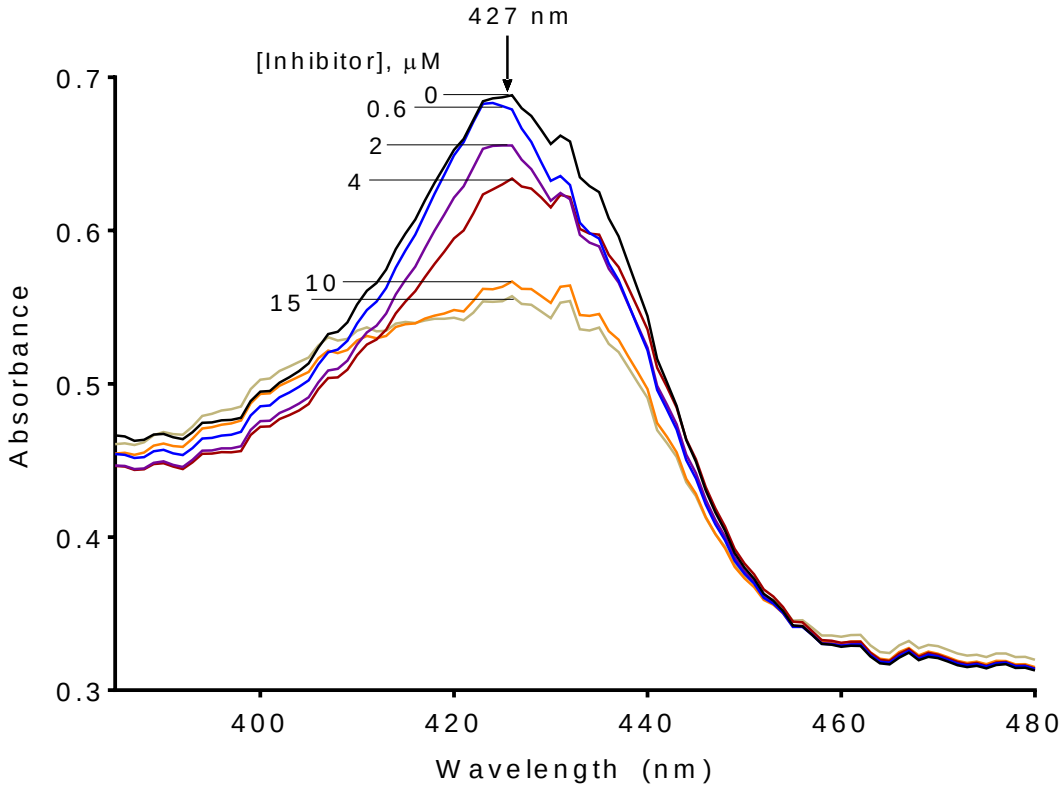

Figure 2, panel B. Ferric hIDO1 in the Presence of Oxygen

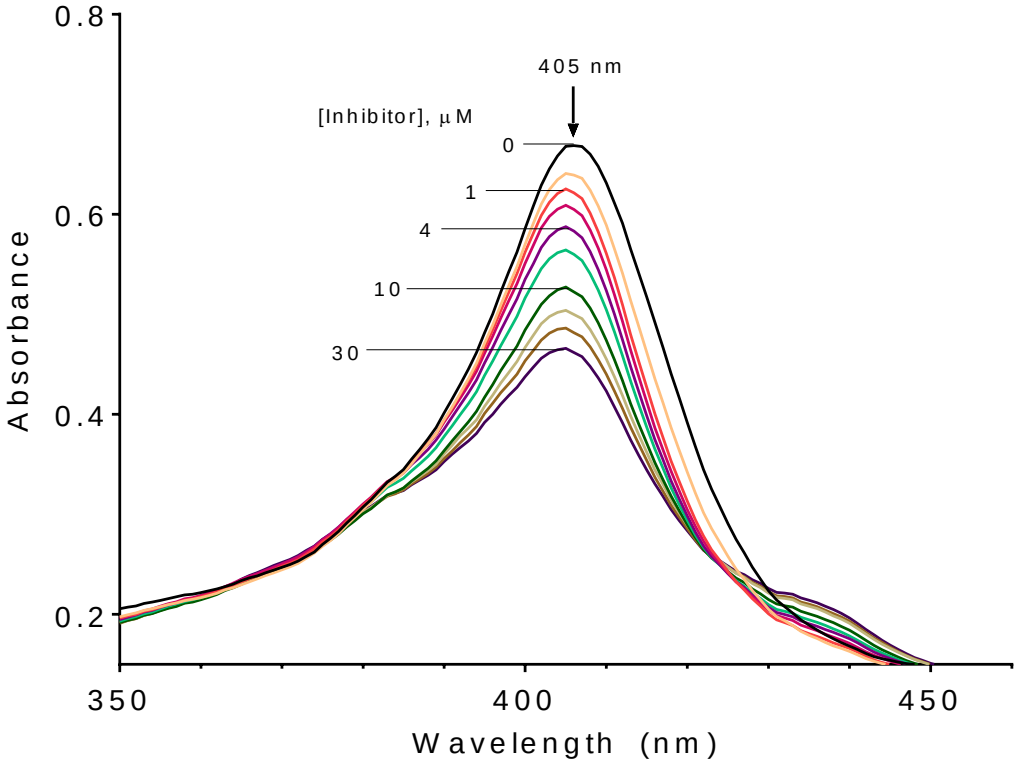

Figure 2, panel C. Ferric hIDO1 after Oxygen Depletion

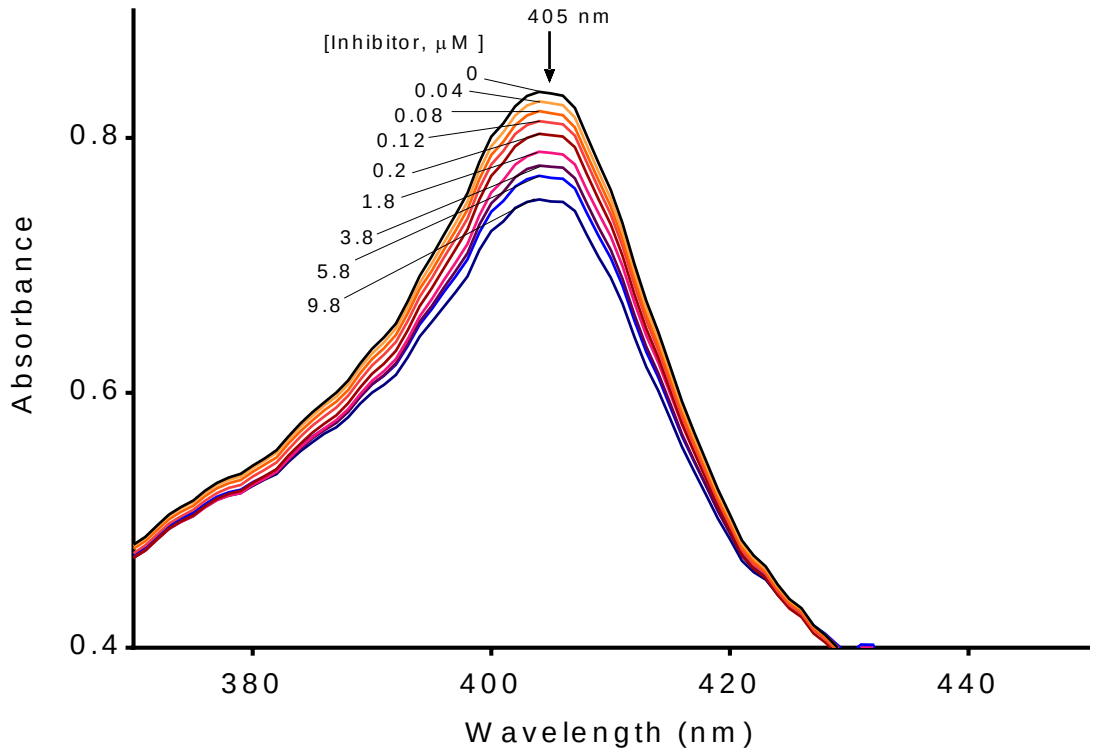

Figure 2, panel D. Ferric hIDO1 plus Tryptophan, after Oxygen Depletion

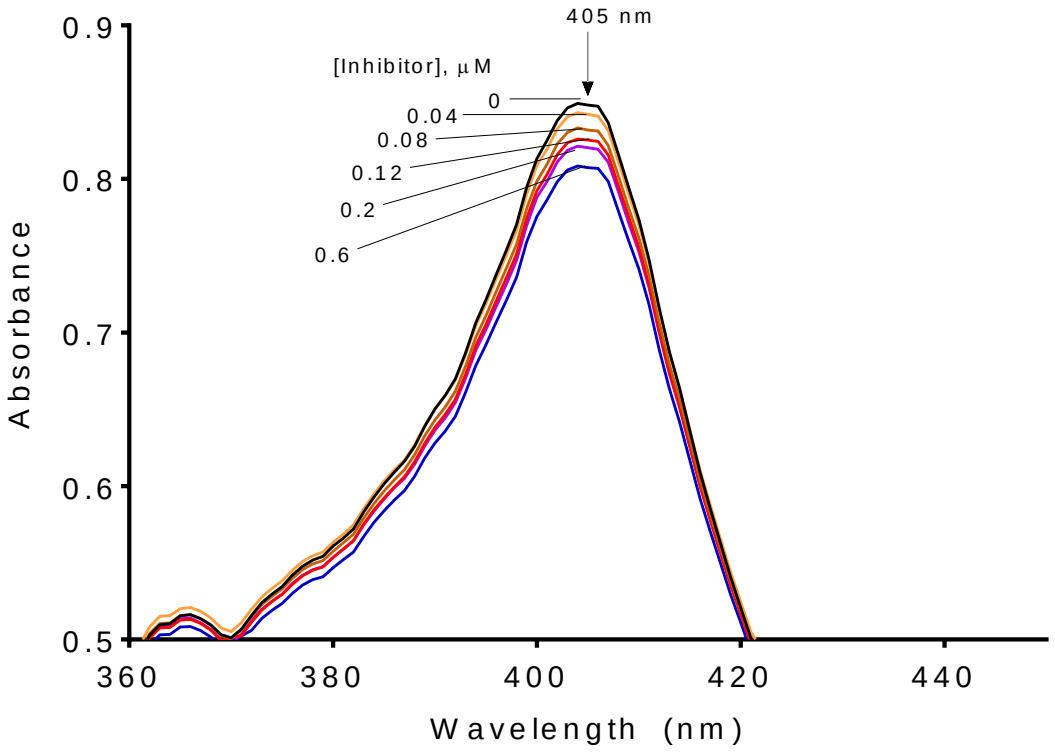

To confirm this binding mode hypothesis, and to map the interactions between **6a** and hIDO-1, an X-ray of the **6a**-IDO-1 complex was obtained (Figure 3, PDB accession code 5WHR). This structure shows that the succinimide ring of **6a** sits parallel to the heme, at a short distance from it, displacing the apical water molecule, while the indole ring lies in the lipophilic pocket. There is no direct interaction between **6a** and the iron atom, despite the close spatial proximity, which justifies the absence of an apical water molecule. Remarkably, all four heteroatoms of **6a** participate in hydrogen-bonding. The indole NH interacts with side chain of Ser167, while the succinimide NH hydrogen bonds to the heme carboxylic acid which adopts a different rotomer compared to other IDO-1 structures in the PDB. The two carbonyls interact to the main chain NH of Ala264 and Thr379. Indeed, residues 376-383 adopt a unique conformation in the **6a** bound structure by forming a loop that folds up to close off the binding pocket and positions Thr379 to

interact with the ligand (Figure 3, loop residues highlighted in dark blue C□ trace). In addition to the hydrogen bond interactions, several aromatic groups (Tyr126, Phe163, Phe164) are appropriately positioned to give π-π interactions with the indole aromatic core. Additional lipophilic residues also are in close contact with the indole group (Leu234, Val130, Cys129).

The very tight packing of the molecule within the IDO-1 active site clearly explains the lack of activity of most of the analogues bearing larger substituents around the indole, as well as the challenge to change any of the succinimide features. Quaternarization of the chiral carbon, which would avoid racemization, is also prevented by its closeness to the heme.

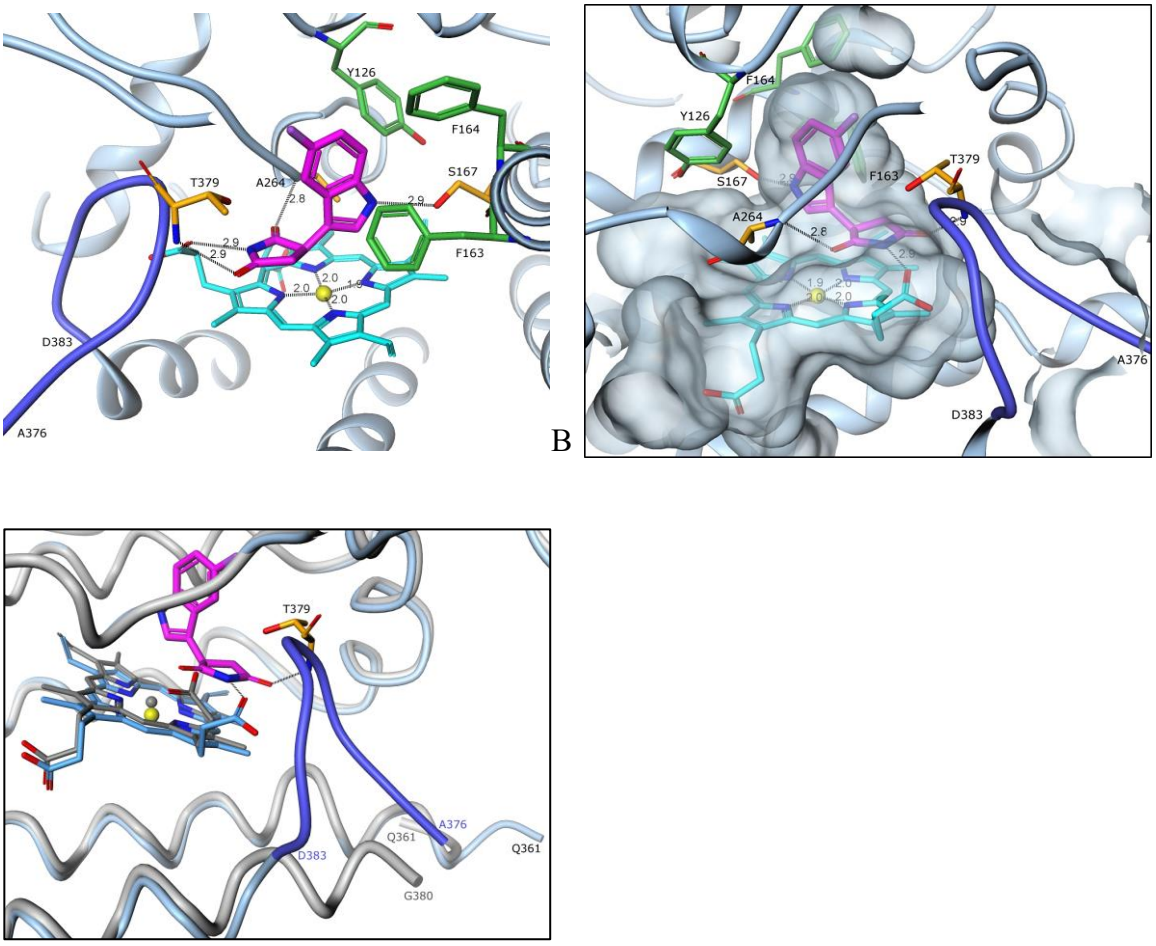

Figure 3. 2.28Å X-ray structure of the complex hIDO-1-**6a.** Protein is represented in light blue Cα trace with key interacting residues in orange and green stick representation. The ligand, **6a**, is drawn in magenta and the heme in cyan stick representation. **(A)** Shows the key hydrogen bond interactions; **(B)** Connolly surface of the protein is shown in grey highlighting the closed binding pocket as a result of the unique ordering of loop A376-D383 (dark blue Cα trace). **(C)** Superposition of the crystal structure of IDO-1 bound to **6a** versus PDB IDO-1 structure 5EK3 (grey Cα trace with grey heme in stick representation, ligand removed for clarity). The unique conformation of residues 376-383 which form a loop in the **6a** bound structure are shown in dark

blue Cα trace. Also shown is the different rotomer adopted by the heme carboxylic acid to interact with the succinimide NH of **6a**.

To confirm activity of **6** and **6a** on the hIDO-1 enzyme, a new assay was developed, using a more sensitive high-throughput mass spectrometry assay which monitors tryptophan and kynurenine. The new assay format allowed us to use lower concentrations of enzyme (1.5 nM) and to have better reproducibility. The IC_{50}s of **6** and **6a** in this assay were 0.40 and 0.20 μM, respectively; whereas the other enantiomer **6b** had much weaker affinity for hIDO1 with an IC_{50} of 38 μM. Compounds **6** and **6a** were found to be less active on the mouse enzyme (IC_{50} 1.5 and 7.3 μM, respectively), whereas the activity on dog IDO-1 was more similar to human IDO-1 (IC_{50} 0.59 and 0.20 μM). Compound **6** was found to have very weak activity against hTDO-2, with an IC_{50} of 140 μM.

In cellular assays, **6** and **6a** were first tested in the classical hIDO-1 HeLa assay:[10] HeLa cells are well known to produce hIDO-1 after stimulation with interferon gamma (INFγ). Incubation of the cells for 24 h after stimulation produces significant levels of kynurenine. In addition to the HeLa cell system, **6** and **6a** were also tested using a second cellular assay based on THP1 (acute monocytic leukemia) cells, to test the effect on a cell line derived from a myeloid-derived cell line. In these cellular assays, **6** and **6a** showed activity both in the HeLa assay (IC_{50} 1.8 and 1.0 μM respectively), as well as in the LPS/INFγ-stimulated THP1 cells (IC_{50}1.7 and 1.1 μM).

Table 3. Summary of *In Vitro* Pharmacology Data for **6** and **6a**

	6	**6a**
hIDO-1 IC_{50} (LCMSMS method, μM)	0.41	0.20

mIDO-1 IC_{50} (LCMSMS method, μM)	1.5	7.3
dIDO-1 IC_{50} (LCMSMS method, μM)	0.59	0.20
HeLa cell IC_{50} (μM)	1.8	1.0
THP1 cell IC_{50} (INFγ/LPS, μM)	1.7	1.1
hTDO-2 IC_{50} (μM)	>50	>50
Whole Blood IC_{50} (μM)	4.7 (total)	2.5 (total) 1.1 (unbound)

Interestingly, we also observed a significant activity of enantiomer **6b** in the HeLa assay (IC_{50} 13 μM), with only a 13-fold difference in potency between the two enantiomers, compared to a 190-fold difference in activity in the enzymatic assay. Considering that the chiral center of **6** is an enolizable carbon, this was interpreted as a sign that significant racemization of the compound could be happening in the conditions of the cellular assay, but not of the enzymatic assay.

As reported in more detail elsewhere[16] compounds **6** and **6a** were also tested in a human whole blood assay: in this assay, whole blood from healthy volunteers, in presence of different concentrations of inhibitors, is treated with INFγ and LPS to induce IDO-1. After 24h, the kynurenine produced can be measured by LCMSMS. The presence of full plasma and red blood cells makes this assay more physiologically relevant, as plasma protein binding and red blood cell distribution will affect the potency of the compound, so that only the unbound fraction of each compound can really inhibit the target. The assay was repeated on 9 different donors, to account for differences due to any possible difference in immune status or metabolism of each individual donor. Despite the moderate potency in isolated cell systems, the low protein binding makes the **6** and **6a** maintain a good efficiency in the whole blood assay, with IC_{50} of

respectively 4.7±2.4 μM and 2.5±1.5 μM. Compound **6** was tested against hIDO2 and it is inactive up to 200 μM. The individual enantiomers were not tested due to very limited enzyme supply.

As reported in more detail elsewhere[15] compounds **6** was evaluated for target selectivity, cardiovascular effects, and genotoxic potential in a series of in vitro assays. To assess the off-target binding potential **6** was tested at a concentration of 200 μM in a CEREP Wide Ligand Profile Screen, where it showed good selectivity.[15] The potential for cardiovascular impact, specifically QT prolongation, was tested using the hERG assay, where **6** showed less than a 50% inhibition of the hERG channel up to 300 μM

ADME. Although **6a** showed optimal ADME properties similar to those of **5a**, it was rapidly converted to the inactive enantiomer **6b** in buffer and plasma of preclinical species and humans. Studies of **6a** with phosphate buffer (pH 7.4) and plasma from animal species were conducted to assess the degree of inter-conversion of **6a** to **6b** (Table 4). While the conversion of **6a** to **6b** was minimal in phosphate buffered saline (pH of 7.4), racemization seemed to be rapid in plasma of preclinical species and humans (Table 4, Figures 4a and 4b). For example, 65% of **6b** was produced in 6 hr, when **6a** was incubated with plasma from humans (Figure 4b). Rapid inter-conversion in the plasma relative to phosphate buffer suggested a possibility of an enzyme catalyzed process.

Interestingly, the ratio of the two enantiomers in human plasma at 48 h was not at the theoretical level of 1:1 irrespective of which enantiomer was present at T0. This was attributed to higher free fraction of **6a** (fup 0.449) relative to **6b** (fup 0.286). When corrected for protein binding, the ratio

of the free fractions of the two enantiomers after 48 h incubations were reasonably close to the theoretical 1:1 ratio.

Table 4. Racemization Experiment: Formation of **6a**/**6b** After Incubation for 48 h of **6a** in Various Biological Media

Matrices	**6a** Remaining (%)	**6b** Formed (%)
Phosphate buffered saline (pH 7.4)	89	11
Mouse Plasma	35	65
Dog Plasma	30	70
Rat Plasma	27	76
Acidified Plasma[1]	93.5	6.6

[1] Dog plasma was acidified

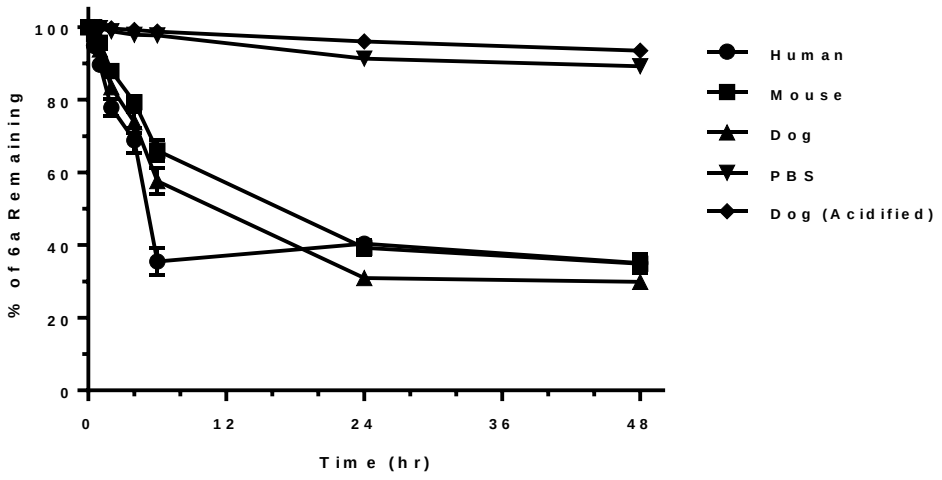

Figure 4a. Time-dependent racemization of **6a** in plasma across species and phosphate-buffered saline (PBS).

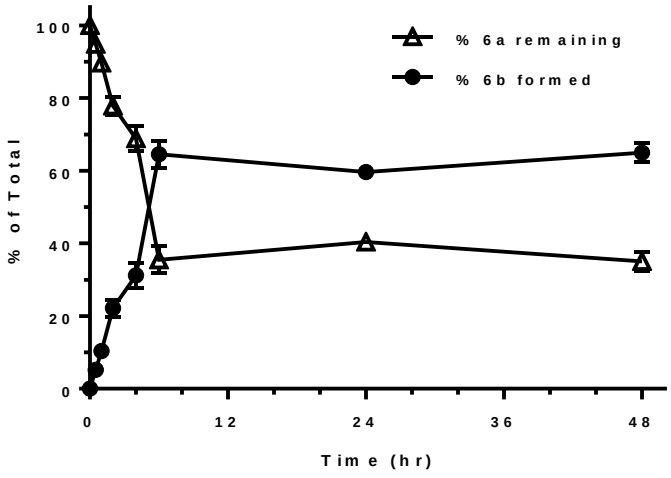

Figure 4b. Time-dependent racemization of **6a** in human plasma. Concentrations of **6a** (empty triangles) and **6b** (filled circles) are measured using a chiral LC/MS-MS method

The low inter-conversion barrier negated the benefits of using single enantiomer for further in vivo biological testing and characterization of the pure enantiomer (**6a**). Advancing the racemate instead of the pure enantiomer was further justified since conversion of **6a** to **6b** was also observed in vivo in all species following an IV dose of **6a** (Table 5). In fact the exposure of **6a** after oral administration of either **6a** or **6** to cynomolgus monkeys suggested only a 20% difference in the exposure of **6a** as depicted in Figure 5. Rapid racemization of **6a** both in vitro and in vivo also justified the advancement of the racemate **6** rather than the active enantiomer **6a** into humans.

Table 5. Exposure (AUCinf) of **6a** and **6b** after intravenous administration (dose, 1 mg/kg) of the active enantiomer **6a** in rat, dog and monkey.

	Rat	Dog	Monkey
in vivo AUC **6a** (h*ng/ml)	2274	696	6808
in vivo AUC **6b** (h*ng/ml)	153	124	3516
in vivo ratio AUC **6b** / AUC **6a**	0.067	0.22	0.52

A 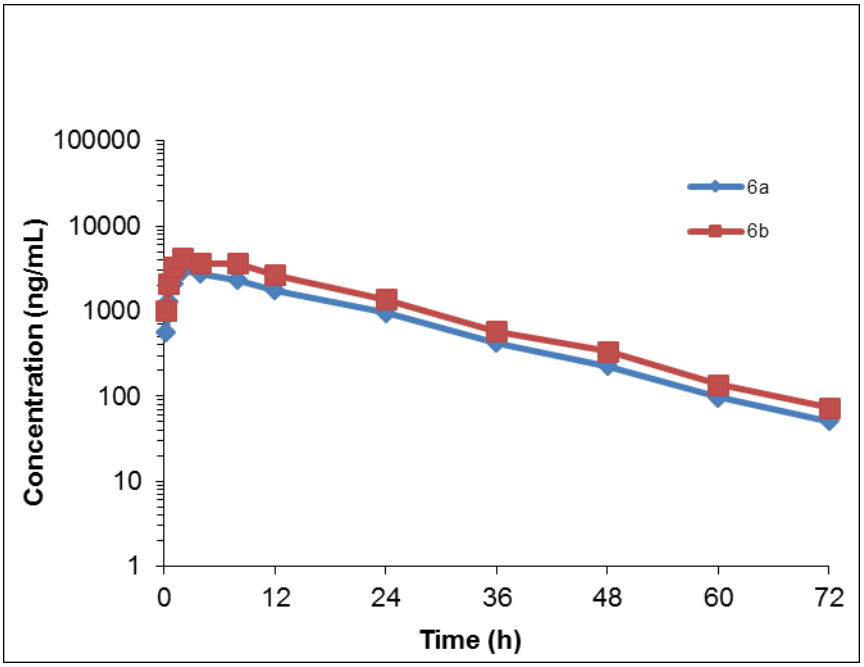

B 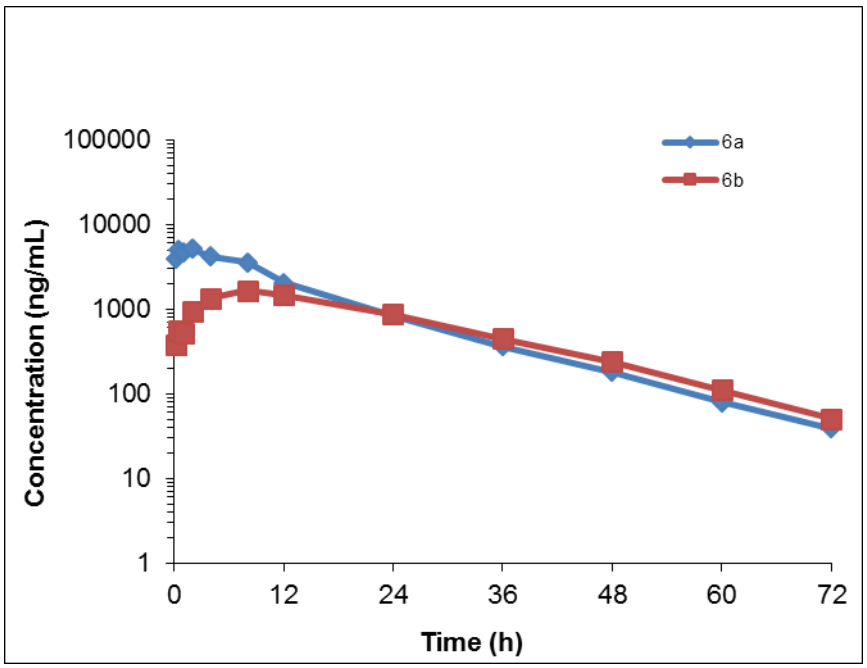

Figure 5. Total concentrations of **6a** (blue diamonds) and **6b** (red squares) dosing of either **6** (panel A) or **6a** (panel B) in monkey (PO dosing at 10 mg/kg)

Consequently, the pharmacokinetics of the active enantiomer (**6a**) was evaluated after single IV administration of the racemic mixture **6** in CD 1 mice, Wistar Han rats and beagle dogs followed by quantitation of the active enantiomer using a chiral LC-MS/MS assay. After a single 1 mg/kg IV dose of **6**, the mean CLp, Vss, and t½ of **6a** was 7.2 mL/min/kg, 0.79 L/kg, and 1.3 hours, respectively, in mouse and 3.4 mL/min/kg, 0.64 L/kg, and 2.2 hours, respectively, in rat. In dogs, the CLp, Vss, and t½ of **6a** following a 1 mg/kg IV dose of **6** was 20 ml/min/kg, 0.96 L/kg, and 0.80 hours, respectively (Table 6; Figure 6).

Table 6: Mean Pharmacokinetics of **6a** in Mouse, Rat, Dog, and Monkey Following Intravenous Administration of **6**.

Species	Sex/n	Dose (mg/kg)	AUC_{inf} (ng-hr/kg)	CL_p (mL/min/kg)	V_{ss} (L/kg)	$T_{1/2}$ (hr)
CD-1 Mouse	Male/3	1	1160	7.21	0.787	2.5
Wistar-Han Rat	Male/3	1	2520	3.44	0.639	2.22
Beagle Dog	Male/3	1	423	20.0	0.957	0.802

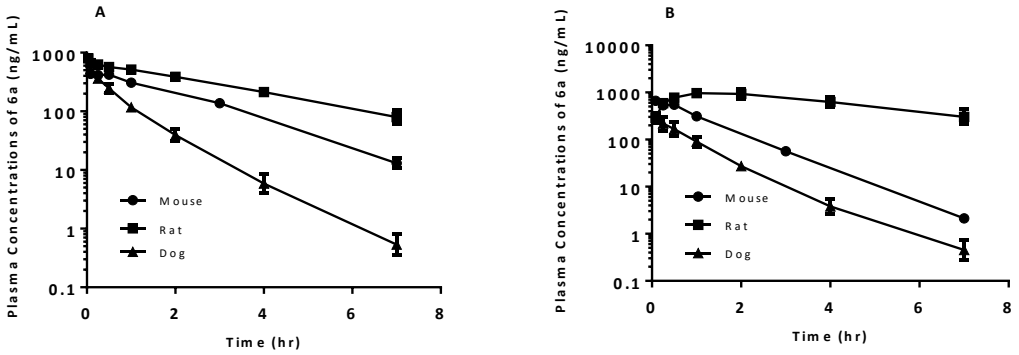

Figure 6: Plasma profile of **6a** following A) an intravenous dose (1 mg/kg) and B) oral dose (3 mg/kg) of the racemate **6** to CD-1 mouse, Wistar-Han rat and Beagle dog.

These results suggested that **6a** exhibited a low plasma clearance (CLp) in the mouse and rat, and moderate CLp in the dog with a low volume of distribution (Vss) in these species (Table 6). Low clearance of **6a** in mouse and rat and moderate to high clearance in the dog was consistent with the projected hepatic clearance values estimated from in vitro incubation of **6** with hepatocytes from the preclinical species (Table 7).

Table 7. Projection of Hepatic Clearance (CL_{hep}) of **6** Following Incubation with Hepatocytes

Species	Clint app μL/min/10^6 cells	CL_{hep} (mL/min/kg)	*In Vivo* CL_{blood}[1] (mL/min/kg)
Rat	2.3	2.9	3.7
Dog	10.3	16.6	24.3
Mouse	2.4	4.5	8.4

1. In vivo CL_{blood} was estimated from the ratio of CL_{plasma} of **6a** (Table 6) and blood to plasma ratio (B/P) for mouse rat and dog which was 0.863, 929 and 0.824, respectively.

Absorption of **6a** was assessed after oral administration of the racemate **6** to CD-1 mice, Wistar-Han rat and Beagle dog. Compound 6a was rapidly absorbed in all three preclinical species when the racemate **6** was dosed at 3 mg/kg as indicated by the time to reach maximum concentration (T_{max}) ranging from 0.25 to 1.3 hours. Oral bioavailability in the mouse and rat was 59 and 94% respectively, and 19% in the dog (Table 8).

Table 8: Mean Pharmacokinetics of **6a** in Mouse, Rat, Dog, and Monkey Following Oral Administration of **6.**

Species	Sex/n	Dose (mg/kg)	C_{max} (ng/mL)	T_{max} (hour)	AUC_{inf} (ng•hr/mL)	$t_{½}$ (hour)	F (%)
CD-1 Mouse	Male/3	3	538	0.58	2170	2.48	59.3
Wistar Han Rat	Male/3	3	985	1.30	6940	2.42	94.0
Beagle Dog	Male/3	3	219	0.25	237	0.840	18.6

The product of fraction absorbed and fraction of **6a** escaping the gut (fa × fg) was calculated using the equation 1;

$$F = f_a \, x \, f_g \, x \, (1 - \frac{CL}{Q}) \quad \text{Equation 1}$$

where F, bioavailability; fa, the fraction absorbed from the GI tract; fg, the fraction escaping metabolism in the intestine; CL, the blood clearance which was estimated from CLp and blood to plasma ratio in the appropriate species and Q, the hepatic blood flow (mouse, 90 ml/min/kg; rat, 70 ml/min/kg and dog, 40 ml/min/kg) and ranged from ~0.5 to 0.99 (mean fa x fg was computed to be 0.70). Good absorption in vivo was consistent with the in vitro permeability assessment of **6** in Ralph-Russ canine kidney (RRCK) cells which demonstrated high intrinsic permeability with an apical to basal ($P_{app\ A\text{-}B}$) value of 25.5 x 10^{-6} cm/sec. Further in vitro studies in Madin –Darby canine kidney (MDCK) cells transfected with the multi-drug resistance gene (MDCK-MDR) that encodes for human Pgp showed minimal evidence of efflux [(basolateral to apical/apical to basolateral (BA/AB) efflux ratio <1.2 up to concentrations of 10 μM] indicating that **6** (or **6a**) was a very weak substrate Pgp substrate in humans. Based on these in vivo and in vitro results, the absorption of **6a** in humans was anticipated to be good after dosing oral administration of the racemate.

Compound **6a** was weakly bound to plasma proteins and was equally distributed between red blood cells and plasma. The unbound fraction (fu) of **6a** following incubation of the racemate with plasma from preclinical species and humans ranged from 0.25 in the rat to 0.45 in humans while the blood to plasma ratio of **6a** ranged from 0.824 to 1.1 when **6** was allowed to equilibrate between blood and plasma. Assessment of CNS exposure of **6a** in the cerebral spinal fluid (CSF) and brain of rats after oral administration of the racemate **6** indicated that **6a** was a brain penetrant with total brain to plasma ratio (Kp = 0.51) and ratio of free concentrations in the brain (B_u) to free

concentrations in the plasma (P_u), $B_u/P_u = 0.20$. The ratio of CSF to free plasma concentrations ($CSF/P_u = 0.49$).

Investigation into clearance mechanisms indicated that the percentage of unchanged **6a** excreted in the urine and bile of rat and the urine of dog was limited (< 1%) following dosing of **6** suggesting that **6a** was primarily cleared via metabolism in preclinical species. Preliminary in vitro metabolism studies with **6** in hepatocytes from mouse, dog, and humans indicated oxidation (hydroxylation) and hydrolysis as the primary routes of metabolism. All metabolites detected in vitro in human hepatocytes were also present in the hepatocytes evaluated from the preclinical species. CYP phenotyping studies with **6a** in cryopreserved human hepatocytes following incubation with and without 1-aminobenzotriazole (ABT), a non-specific CYP enzyme inhibitor, suggested that CYP450 dependent metabolism accounted for approximately 61% of the metabolic turnover and non-CYP450 dependent hydrolytic metabolism accounted for 39%. Incubation with specific inhibitors of the major CYP isoforms indicated that CYP1A2 was the primary isozyme that was responsible for oxidative metabolism of **6a**.

Inhibition and induction studies with primary CYP isoforms and major efflux transporters were conducted to assess the risk of pharmacokinetic drug interactions. These studies revealed that **6** was a very weak inhibitor of CYPs with IC_{50} values greater than 100 μM for most major CYP isozymes except 2C19 (IC_{50} value was 78 μM). Additionally, **6** did not exhibit metabolism dependent (time-dependent and NADPH-dependent) or time dependent (NADPH-independent) inhibition of the major CYP enzymes investigated. Likewise, in vitro experiments to investigate the potential for **6** to inhibit P-gp or BCRP mediated transport of digoxin and pitavastatin as known P-gp and BCRP substrates in MDCK-MDR or MDCK-BCRP cells indicated an IC_{50} of >300 μM and 65.4 μM, respectively, suggesting weak inhibition of these transporters as well. Similarly, **6**

was a weak inducer of CYP enzymes. Treatment of human hepatocytes with **6** did not cause induction of CYP1A2, 3A4 or 2B6 messenger ribonucleic acid (mRNA) below 100 μM concentrations.

Projection of PK parameters in humans

Since excellent in vitro and in vivo correlations were observed between clearances scaled from hepatocyte data and in vivo clearances of the preclinical species, estimation of hepatic clearance using human hepatocytes was considered to be an appropriate method for the projection of human clearance. The intrinsic clearance of **6a** after incubation of **6** with human hepatocytes was also low (0.58 μl/min/ 10^6 cells) and resulted in projected hepatic clearance of 0.60 mL/min/kg (CLp = 0.64 ml/min/kg) (Table 9).

Table 9. Projected Pharmacokinetic parameters of **6a** following oral administration of the racemate **6.**

Compound	CL_p mL/min/kg	Vd_{ss} L/Kg	$T_{1/2}$ hr	F %
6a	0.64	1.1	19	64

As noted earlier, distribution of the **6a** after administration of **6** to preclinical species was low to moderate in all species given that Vdss of **6a** ranged from 0.639 to 0.957 L/kg. The apparent volume of distribution in humans of a compound is generally more related to the molecular properties of the compound and thus, this parameter is more successfully predicted by scaling the apparent Vdss obtained from PK data in animals and unbound bound fraction in human plasma. Using this approach, the projected human Vdss ranged from 0.90 to 1.19 L/kg resulting with a mean Vdss of 1.03 L/Kg. In summary, after oral administration of **6**, **6a** had a predicted CL_p of

0.64 ml/min/kg and a V_{ss} of 1.03 L/kg in humans yielding a half-life ($t_{½}$) of approximately 19 hours suggesting once to twice a day dosing regimen (Table 9). The bioavailability of **6a** in humans following oral administration of **6** was projected assuming that the fa x fg of **6a** in the humans following oral dosing of **6**, is similar to that in monkeys. Since the exposure of **6a** following oral administration of **6** was only 20% lower than that achieved when the active enantiomer (**6a**) was orally administered, the fa x fg of **6a** following oral administration of **6** was estimated to be 0.67. Using this estimation in equation 1, the bioavailability (F) of **6a** was estimated to be 64% (Table 9).

As reported in more detail elsewhere[15] compound **6** modulated hIDO-1 activity in non-tumor bearing mice as determined by the strong maximum reduction in plasma L-kynurenine (≥ 54 ± 6%) observed at or above 200 mg/kg 1 hour post treatment.. In addition, **6** has shown significant anti-tumor activity in monotherapy in Pan02, B16-F10, CT26, MC38, 4T1 and Renca models ($p<0.05$ vs Vehicle-treated group) and very good synergy in combination with anti-PDL1 mAb in CT26 model ($p<0.05$ vs monotherapy groups).[25]

Conclusion

3-(5-Fluoro-1*H*-indol-3-yl)pyrrolidine-2,5-dione **6** (EOS200271/PF-06840003)[26] is a novel class of hIDO-1 inhibitor, not relying on coordination to the heme iron for achieving inhibition. Although it has moderate hIDO1 enzyme inhibition (IC_{50} 0.41μM), it is a highly efficient compound (LE 0.53, LipE 5.1), driven by its tight packing within the enzyme, as well as the high density of hydrogen bonds it forms with hIDO-1 despite its small size. While the affinity of the compound for hIDO-1 is not as high as for other hIDO-1 inhibitors, its low plasma protein binding (f_u 0.45) gives it good potency in the more physiologically relevant human whole blood

assay. The PK profile of the compound is excellent, with a low/moderate clearance in most preclinical species. Human PK predictions are promising, and after oral administration of **6**, **6a** has a predicted CLp of 0.64 ml/min/kg and a Vss of 1.03 L/kg with a t½ ≈ 19 hours, which should allow QD administration. The bioavailability of **6a** after an oral dose of **6** is projected to be 64%. The compound also shows good CNS penetration in rat, suggesting potential impact on brain metastases. Based on this favorable profile, **6** was selected to advance to clinical trials and a First in Patient Study in Malignant Gliomas ((NCT02764151).

Experimental Section

The MS data were obtained using an Agilent 6110 (ESI) or a Waters Acquity SQD (ESI). The NMR data were obtained as followed: Bruker Ultrashield ™ 400 PLUS and Bruker Fourier 300 MHz and TMS was used as an internal standard. Purity for all final compounds was determined by HPLC, and was generally >95%. Analytical HPLC method A: XbridgeTM C8 50 mm x 4.6 mm at a flow of 2 mL/min; 8 min gradient from 0.1 % TFA in H2O to 0.07 % TFA in CH3CN. The microwave chemistry was performed on a single mode microwave reactor Initiator Microwave System EU from Biotage. Preparative HPLC purifications were performed with a mass directed autopurification Fractionlynx from Waters equipped with a Xbridge™ Prep C18 OBD column 19x150 mm 5 µm, unless otherwise reported. All HPLC purifications were performed with a gradient of $CH_3CN/H_2O/NH_4HCO_3$ (5 mM), CH_3CN /H_2O/TFA (0.1%), or CH_3CN /H_2O/NH_3 H_2O (0.1%).

General protocol for the synthesis of 3-(indol-3-yl)pyrrolidine-2,5-diones

A mixture of indole (2.22 mmol), maleimide (646 mg; 6.65 mmol) in AcOH (2 mL) was stirred at 170 °C for 2 h in a microwave reaction. The reaction mixture was concentrated in vacuo. The residue was neutralized with saturated aqueous NaHCO3 solution to pH 7~8 and extracted with EtOAc (10 mL×3). The combined organic layers were dried over anhydrous Na2SO4, filtered, concentrated, and purified by preparative HPLC to afford the product.

The following compounds were prepared according to the protocol above:

3-(1*H*-Indol-3-yl)pyrrolidine-2,5-dione (**5**)

LC-MS for $C_{12}H_{10}FN_2O_2$+H^+ $[M+H]^+$: calcd. 215.1; found: 215.1. ^{1}H NMR (400 MHz, DMSO-d6) δ [ppm]: 11.29 (s, 1H), 11.02 (s, 1H), 7.42 (d, *J* = 8.0 Hz, 1H), 7.39 (d, *J* = 8.1 Hz, 1H), 7.32 (d, *J* = 2.4 Hz, 1H), 7.12-7.07 (m, 1H), 7.02 – 6.97 (m, 1H), 4.33 (dd, *J* = 9.5, 5.3 Hz, 1H), 3.18 (dd, *J* = 18.0, 9.5 Hz, 1H), 2.76 (dd, *J* = 18.0, 5.3 Hz, 1H).

3-(5-Fluoro-1*H*-indol-3-yl)pyrrolidine-2,5-dione (**6**)

Prepared according to the protocol described for compound **5**.

LC-MS for $C_{12}H_9FN_2O_2$-H- [M-H]: calcd. 231.1; found: 231.0. ^{1}H NMR (300 MHz, DMSO-d6) δ [ppm]: 11.30 (brs, 1H), 11.14 (s, 1H), 7.41(d, *J* = 2.5 Hz, 1H), 7.36 (dd, *J* = 9.0, 4.6 Hz, 1H), 7.20 (dd, *J* = 10.1, 2.5 Hz, 1H), 6.94 (ddd, *J* = 9.2, 9.0, 2.5 Hz, 1H), 4.33 (dd, *J* = 9.5, 5.5 Hz, 1H), 3.17 (dd, *J* = 18.0, 9.5 Hz, 1H), 2.79 (dd, *J* = 18.0, 5.5 Hz, 1H).

Alternative protocol for the synthesis of **6**. A mixture of 5-Fluoroindole (5.00 g, 35.5 mmol) and Maleimide (1.5 equiv., 5.17 g, 53.3 mmol) was charged in a 50 mL vessel, and then Acetonitrile

(15.0 mL) and Zinc Chloride (1.05 equiv., 5.08 g, 37.3 mmol) were added. The reaction was heated to 85 °C over 10 min and then maintained at 85 °C for 24 hrs. While still at 85 °C, Water (30 mL) was added slowly, while maintaining the tempearture above 80 °C. Yellow solids precipitated. The reaction mixture was cooled to 50 °C over 1 hour followed by stirring at 50 °C for 2 hours, then cooled to 10 °C over 1 hour. The reaction was stirred at 10 °C for 1 hour, then the solids were filtered off and the filter cake was washed 2 times with 5 ml 1:1 ACN/water to afford isolated compound (6.85 g, 6.85 g, 29.5 mmol, 83.1% Yield). For purification, the resulting isolated compound was charged into a vessel, followed by addition of Tetrahydrofuran (41 mL). This mixture was heated to 66 °C to form a homogeneous solution. Heptane (27.4 mL) was added slowly at 66 °C. The mixture was cooled to 25 °C over 3 hours, then filtered and washed with heptane, followed by drying in in the high vacuum oven overnight to afford **6** (4.93 g, 72.0% Yield).

3-(5-Chloro-1*H*-indol-3-yl)pyrrolidine-2,5-dione (**7**)

Prepared according to the protocol described for compound **5**.

LC-MS for $C_{12}H_9ClN_2O_2$-H^- $[M-H]^-$: calcd. 247.0; found: 247.0. ^{1}H NMR (300 MHz, DMSO-d6) δ [ppm]: 11.30 (br s, 1H), 11.25 (br s, 1H), 7.49 (d, J = 2.0 Hz, 1H), 7.42 (d, J = 2.0 Hz, 1H), 7.39 (d, J = 8.6 Hz, 1H), 7.10 (dd, J = 8.6, 2.0 Hz, 1H), 4.36 (dd, J = 9.5, 5.5 Hz, 1H), 3.17 (dd, J = 18.0, 9.5 Hz, 1H), 2.80 (dd, J = 18.0, 5.5 Hz, 1H).

3-(5-Bromo-1*H*-indol-3-yl)pyrrolidine-2,5-dione (**8**)

Prepared according to the protocol described for compound **5**.

LC-MS for $C_{12}H_9BrN_2O_2+H^+$ $[M+H]^+$: calcd. 293.0; found: 293.0. ^{1}H NMR (400 MHz, DMSO-d6) δ [ppm]: 11.29 (s, 1H), 11.26 (s, 1H), 7.64 (d, *J* = 1.8 Hz, 1H), 7.40 (d, *J* = 2.4 Hz, 1H), 7.35 (d, *J* = 8.6 Hz, 1H), 7.21 (dd, *J* = 8.6, 1.8 Hz, 1H), 4.36 (dd, *J* = 9.5, 5.5 Hz, 1H), 3.17 (dd, *J* = 18.0, 9.5 Hz, 1H), 2.80 (dd, *J* = 18.0, 5.5 Hz, 1H).

3-(2,5-Dioxopyrrolidin-3-yl)-1*H*-indole-5-carbonitrile (**9**)

Prepared according to the protocol described for compound **5**.

A mixture of 3-(5-bromo-1*H*-indol-3-yl)pyrrolidine-2,5-dione (**8**; 500 mg; 1.71 mmol) and CuCN (231 mg; 2.58 mmol) in NMP (3 mL) was stirred at 200 °C for 1.5 h in a microwave reactor. The reaction mixture was purified by preparative HPLC to afford the product (110 mg; 27%) as a green solid.

LC-MS for $C_{13}H_9N_3O_2+H^+$ $[M+H]^+$: calcd. 240.1; found: 240.1. ^{1}H NMR (300 MHz, DMSO-d6) δ [ppm]: 11.63 (brs, 1H), 8.04 (s, 1H), 7.57 (d, *J* = 1.8 Hz, 1H), 7.54 (d, *J* = 8.8 Hz, 1H), 7.45 (dd, *J* = 8.6, 1.8 Hz, 1H), 4.44 (dd, *J* = 9.5, 5.8 Hz, 1H), 3.18 (dd, *J* = 17.8, 9.5 Hz, 1H), 2.87 (dd, *J* = 17.8, 5.8 Hz, 1H).

3-(5-Methoxy-1*H*-indol-3-yl)pyrrolidine-2,5-dione (**10**)

Prepared according to the protocol described for compound **5**.

LC-MS for $C_{13}H_{12}N_2O_3+H^+$ $[M+H]^+$: calcd. 245.1; found: 245.1. ^{1}H NMR (400 MHz, DMSO-d6) δ [ppm]: 11.25 (brs, 1H), 10.86 (s, 1H), 7.27 (d, *J* = 2.2 Hz 1H), 7.26 (d, *J* = 8.6 Hz, 1H), 6.91 (d, *J* = 2.2 Hz, 1H), 6.76 (dd, *J* = 8.6, 2.2 Hz, 1H), 4.30 (dd, *J* = 9.6, 5.3 Hz, 1H), 3.74 (s, 3H), 3.18 (dd, *J* = 17.9, 9.6 Hz, 1H), 2.75 (dd, *J* = 17.9, 5.3 Hz, 1H).

3-(5-Methyl-1*H*-indol-3-yl)pyrrolidine-2,5-dione (**11**)

Prepared according to the protocol described for compound **5**.

LC-MS for $C_{13}H_{12}N_2O_2+H^+$ $[M+H]^+$: calcd. 229.1; found: 229.1. ^{1}H NMR (400 MHz, DMSO-d6) δ [ppm]: 11.27 (s, 1H), 10.88 (s, 1H), 7.26 (dd, *J* = 8.3, 2.0 Hz), 7.25 (d, *J* = 2.0 Hz, 1H), 7.19 (s, 1H), 6.92 (d, *J* = 8.3 Hz, 1H), 4.29 (dd, *J* = 9.5, 5.3 Hz, 1H), 3.16 (dd, *J* = 18.0, 9.5 Hz, 1H), 2.74 (dd, *J* = 18.0, 5.3 Hz, 1H), 2.36 (s, 3H).

3-(5-Trifluoromethyl-1*H*-indol-3-yl)pyrrolidine-2,5-dione (**12**)

Prepared according to the protocol described for compound **5**.

LC-MS for $C_{13}H_9F_3N_2O_2$-H^- $[M-H]^-$: calcd. 281.2; found: 281.1. ^{1}H NMR (400 MHz, DMSO-d6) δ [ppm]: 11.48 (s, 1H), 11.26 (s, 1H), 7.87 (s, 1H), 7.54 (d, *J* = 8.5 Hz, 1H), 7.53 (s, 1H), 7.36 (d, *J* = 8.5, 1H), 4.44 (dd, *J* = 9.5, 5.5 Hz, 1H), 3.17 (dd, *J* = 18.0, 9.5 Hz, 1H), 2.86 (dd, *J* = 18.0, 5.5 Hz, 1H).

3-(6-Fluoro-1*H*-indol-3-yl)pyrrolidine-2,5-dione (**13**)

Prepared according to the protocol described for compound **5**.

LC-MS for $C_{12}H_9FN_2O_2$-H^- $[M-H]^-$: calcd. 231.1; found: 231.1. ^{1}H NMR (400 MHz, DMSO-d6) δ [ppm]: 11.10 (s, 1H), 7.43 (dd, *J* = 8.7, 5.4 Hz, 1H), 7.33 (d, *J* = 2.0 Hz, 1H), 7.14 (dd, *J* = 10.1, 2.3 Hz, 1H), 6.87 (td, *J* = 9.8, 8.7, 2.3 Hz, 1H), 4.34 (dd, *J* = 9.5, 5.4 Hz, 1H), 3.17 (dd, *J* = 18.0, 9.5 Hz, 1H), 2.77 (dd, *J* = 18.0, 5.4 Hz, 1H).

3-(6-Chloro-1*H*-indol-3-yl)pyrrolidine-2,5-dione (**14**)

Prepared according to the protocol described for compound **5**.

LC-MS for $C_{12}H_9ClN_2O_2$-H^- $[M-H]^-$: calcd. 247.0; found: 247.0. ^{1}H NMR (300 MHz, DMSO-d6) δ [ppm]: 11.27 (brs, 1H), 11.17 (s, 1H), 7.45 (d, *J* = 8.4 Hz, 1H), 7.41 (d, *J* = 1.8 Hz, 1H), 7.38 (d, *J* = 2.4 Hz, 1H), 7.03 (dd, *J* = 8.4, 1.8 Hz, 1H), 4.34 (dd, *J* = 9.5, 5.5 Hz, 1H), 3.17 (dd, *J* = 18.0, 9.5 Hz, 1H), 2.77 (dd, *J* = 18.0, 5.5 Hz, 1H).

3-(6-Bromo-1*H*-indol-3-yl)pyrrolidine-2,5-dione (**15**)

Prepared according to the protocol described for compound **5**.

HPLC. LC-MS for $C_{12}H_9BrN_2O_2$+H^+ $[M+H]^+$: calcd. 293.0; found: 293.0. ^{1}H NMR (300 MHz, DMSO-d6) δ [ppm]: 11.30 (brs, 1H), 11.18 (s, 1H), 7.56 (d, *J* = 1.6 Hz, 1H), 7.41 (d, *J* = 8.5 Hz, 1H), 7.37 (d, *J* = 2.4 Hz, 1H), 7.14 (dd, *J* = 8.5, 1.7 Hz, 1H), 4.34 (dd, *J* = 9.5, 5.4 Hz, 1H), 3.17 (dd, *J* = 18.0, 9.5 Hz, 1H), 2.77 (dd, *J* = 18.0, 5.4 Hz, 1H).

3-(2,5-Dioxopyrrolidin-3-yl)-1*H*-indole-6-carbonitrile (**16**)

Prepared according to the protocol described for compound **5**.

LC-MS for $C_{13}H_9N_3O_2$+H^+ [M+H]+: calcd. 240.1; found: 240.1. ^{1}H NMR (300 MHz, DMSO-d6) δ [ppm]: 11.63 (brs, 1H), 11.32 (s, 1H), 7.88 (s, 1H), 7.68 – 7.62 (m, 2H), 7.35 (dd, *J* = 9.5, 5.6 Hz, 1H), 4.42 (dd, *J* = 17.8, 9.5 Hz, 1H), 3.18 (dd, *J* = 18.0, 9.9 Hz, 1H), 2.82 (dd, *J* = 17.8, 5.6 Hz, 1H).

3-(6-Methoxy-1*H*-indol-3-yl)pyrrolidine-2,5-dione (**17**)

Prepared according to the protocol described for compound **5**.

HPLC. LC-MS for $C_{13}H_{12}N_2O_3$-H^- $[M-H]^-$: calcd. 243.1; found: 243.1. ^{1}H NMR (400 MHz, DMSO-d6) δ [ppm]: 11.26 (s, 1H), 10.81 (s, 1H), 7.29 (d, *J* = 8.7 Hz, 1H), 7.16 (d, *J* = 2.2 Hz, 1H), 6.86 (d, *J* = 2.2 Hz, 1H), 6.66 (dd, *J* = 8.7, 2.2 Hz, 1H), 4.27 (dd, *J* = 9.5, 5.2 Hz, 1H), 3.75 (s, 3H), 3.16 (dd, *J* = 18.0, 9.5 Hz, 1H), 2.73 (dd, *J* = 18.0, 5.2 Hz, 1H).

3-(6-Methyl-1*H*-indol-3-yl)pyrrolidine-2,5-dione (**18**)

Prepared according to the protocol described for compound **5**.

HPLC. LC-MS for $C_{13}H_{12}N_2O_2$-H^- $[M-H]^-$: calcd. 227.1; found: 227.1. ^{1}H NMR (300 MHz, DMSO-d6) δ [ppm]: 10.85 (brs, 2H), 11.18 (s, 1H), 7.28 (d, *J* = 8.0 Hz, 1H), 7.20 (d, *J* = 2.3 Hz, 1H), 7.16 (s, 1H), 6.83 (d, *J* = 8.0 Hz, 1H), 4.28 (dd, *J* = 9.5, 5.3 Hz, 1H), 3.17 (dd, *J* = 18.0, 9.5 Hz, 1H), 2.73 (dd, *J* = 18.0, 5.3 Hz, 1H), 2.38 (s, 3H).

3-(5,6-Difluoro-1*H*-indol-3-yl)pyrrolidine-2,5-dione (**19**)

Prepared according to the protocol described for compound **5**.

LC-MS for $C_{12}H_8F_2N_2O_2$+H^+ $[M+H]^+$: calcd. 251.1; found: 251.0. ^{1}H NMR (300 MHz, DMSO-d6) δ [ppm]: 11.27 (brs, 1H), 11.21 (brs, 1H), 7.45 (dd, *J* = 11.5, 8.0 Hz, 1H), 7.41 (d, *J* = 1.8 Hz, 1H), 7.37 (dd, *J* = 11.2, 7.0 Hz, 1H), 7.48-7.34 (m, 3H), 4.34 (dd, *J* = 9.3, 5.6 Hz, 1H), 3.16 (dd, *J* = 18.0, 9.3 Hz, 1H), 2.80 (dd, *J* = 18.0, 5.6 Hz, 1H).

3-(6-Chloro-5-fluoro-1*H*-indol-3-yl)pyrrolidine-2,5-dione (**20**)

Prepared according to the protocol described for compound **5**.

LC-MS for $C_{12}H_8ClFN_2O_2$-H^- $[M-H]^-$: calcd. 265.1; found: 265.0. ^{1}H NMR (300 MHz, DMSO-d6) δ [ppm]: 11.30 (br s, 1H), 11.27 (br s, 1H), 7.54 (d, *J* = 6.4 Hz, 1H), 7.47 (s, 1H), 7.46 (d, *J* = 10.2 Hz, 1H), 4.35 (dd, *J* = 9.4, 5.8 Hz, 1H), 3.16 (dd, *J* = 18.0, 9.4 Hz, 1H), 2.81 (dd, *J* = 18.0, 5.8 Hz, 1H).

3-(6-Bromo-5-fluoro-1*H*-indol-3-yl)pyrrolidine-2,5-dione (**21**)

Prepared according to the protocol described for compound **5**.

LC-MS for $C_{12}H_8BrFN_2O_2$-H^- $[M-H]^-$: calcd. 309.0; found: 308.9. ^{1}H NMR (300 MHz, DMSO-d6) δ [ppm]: 11.31 (s, 1H), 11.27 (s, 1H), 7.66 (d, *J* = 6.0 Hz, 1H), 7.48 (d, *J* = 1.7 Hz, 1H), 7.44 (d, *J* = 9.8 Hz, 1H), 4.36 (dd, *J* = 9.2, 5.6 Hz, 1H), 3.17 (dd, *J* = 18.0, 9.2 Hz, 1H), 2.82 (dd, *J* = 18.0, 5.6 Hz, 1H).

3-(5-Fluoro-6-methyl-1*H*-indol-3-yl)pyrrolidine-2,5-dione (**22**)

Prepared according to the protocol described for compound **5**.

LC-MS for $C_{13}H_{11}FN_2O_2$+H^+ $[M+H]^+$: calcd. 247.1; found: 247.1. ^{1}H NMR (300 MHz, DMSO-d6) δ [ppm]: 11.28 (s, 1H), 10.99 (s, 1H), 7.31 (d, *J* = 2.5 Hz, 1H), 7.22 (d, *J* = 6.4 Hz, 1H), 7.13 (d, *J* = 10.8 Hz, 1H), 4.29 (dd, *J* = 9.4, 5.4 Hz, 1H), 3.16 (dd, *J* = 18.0, 9.4 Hz, 1H), 2.76 (dd, *J* = 18.0, 5.4 Hz, 1H), 2.30 (d, , *J* = 1.6 Hz, 3H).

3-(Naphthalen-1-yl)pyrrolidine-2,5-dione (**23**)

To a solution of naphthalen-1-ylboronic acid (0.27 g; 1.57 mmol) in 1,4-dioxane (9 mL) and water (1.4 mL) was added Et_3N (0.10 g; 0.99 mmol), [RhOH(cod)]2 (23 mg; 0.05 mmol) and maleimide (100 mg; 1.03 mmol).The dark brown mixture was heated at 50 °C for 2.5 h, cooled

to room temperature, and concentrated in vacuo. The residue was diluted with water (10 mL) and extracted with dichloromethane (20 mL×3). The combined organic layers were dried over anhydrous sodium sulfate, filtered, concentrated, and purified by preparative HPLC to afford 136 mg (59 %) of the title compound as a white solid. LC-MS for $C_{14}H_{11}NO_2$-H^- [M-H]$^-$: calcd. 224.1; found: 224.1. ^{1}H NMR (300 MHz, DMSO-d6) δ [ppm]: 11.50 (s, 1H), 8.02-7.95 (m, 2H), 7.89 (d, *J* = 9.1 Hz, 1H), 7.63 – 7.53 (m, 2H), 7.53 – 7.46 (m, 1H), 7.41 (d, *J* = 7.1 Hz, 1H), 4.96 (dd, *J* = 9.6, 5.7 Hz, 1H), 3.32 (dd, *J* = 18.0, 9.6 Hz, 1H), 2.71 (dd, *J* = 18.0, 5.7 Hz, 1H).

3-(7-Fluoronaphthalen-1-yl)pyrrolidine-2,5-dione (**24**)

Prepared according to the procedure described for compound **25**

LC-MS for $C_{14}H_{10}FNO_2$-H^- [M-H]$^-$: calcd. 242.1; found: 242.0. ^{1}H NMR (300 MHz, MeOH-d4) δ [ppm]: 7.99 (dd, *J* = 9.0, 5.9 Hz, 1H), 7.88 (dd, *J* = 6.8, 2.0 Hz, 1H), 7.70 (d, *J* = 11.1, 2.0 Hz, 2H), 7.50-7.42 (m, 1H), 7.41 – 7.32 (m, 1H), 4.88 (dd, *J* = 9.5, 5.1 Hz, 1H), 3.43 (dd, *J* = 18.2, 9.5 Hz, 1H), 2.72 (dd, *J* = 18.2, 5.1 Hz, 1H).

3-(6-Fluoronaphthalen-1-yl)pyrrolidine-2,5-dione (**25**)

Step 1: 6-fluoronaphthalene-1-diazonium tetrafluoroborate

To a solution of 6-fluoronaphthalen-1-amine (500 mg; 3.10 mmol) and HBF_4 (40 %; 2 mL; 12.6 mmol) in water (2 mL) at 0 °C was added a cold solution of $NaNO_2$ (214 mg; 3.10 mmol) in water (0.5 mL) dropwised. The reaction was stirred at room temperature for 1 h. The precipitate was collected by filtration, washed with ethanol (5 mL), diethyl ether (5 mL), and dried under vacuum to afford 0.40 g (50%) of the title compound as a pale solid, which was used to directly in the next step without further purification.

Step 2: 2-(6-fluoronaphthalen-1-yl)succinic acid

Maleic anhydride (150 mg; 1.54 mmol) was added with to an aqueous NaOH solution (4 M; 0.70 mL; 2.8 mmol). The resulting solution was added at 0-5 °C to an aqueous $TiCl_3$ solution (15%; 3.2 g; 3.11 mmol), followed by acetone (2 mL). The cooling bath was removed and 6-fluoronaphthalene-1-diazonium tetrafluoroborate (Step 1: 400 mg; 1.54 mmol) was added slowly over 0.7 h. The suspension was stirred at room temperature for 1.5 h, concentrated to remove acetone, and extracted with diethyl ether (10 mL×3). The aqueous layer was acidified to pH~1 with hydrochloric acid (1 M) and extracted with ethyl acetate (10 mL×3). The combined organic layers were dried over anhydrous sodium sulfate, filtered, and concentrated to afford 190 mg (47%) of the title compound as a brown solid, which was used directly in the next step without further purification. LC-MS for $C_{14}H_{11}FO_4$+NH_4^+ $[M+ NH_4]^+$: calcd. 280.1; found: 280.0.

Step 3:

A mixture of 2-(6-fluoronaphthalen-1-yl)succinic acid (190 mg; 0.72 mmol) and urea (170 mg; 2.83 mmol) was stirred at 180 °C for 1 h. The reaction mixture was purified by silica gel chromatography (petroleum ether/ehtyl acetate = 1/1) to give a yellow solid, which was further purified by preparative HPLC to afford 63 mg (36%) the title compound as a white solid. LC-MS for $C_{14}H_{10}FNO_2$+H^+ $[M+H]^+$: calcd. 244.1; found:243.9. ^{1}H NMR (300 MHz, DMSO-d6) δ [ppm]: 8.08 (dd, J = 9.3, 5.6 Hz, 1H), 7.87 (d, J = 8.2 Hz, 1H), 7.76 (dd, J = 10.2, 2.7 Hz, 1H), 7.56 – 7.46 (m, 2H), 7.38 (d, J = 6.6 Hz, 1H), 4.95 (dd, J = 9.4, 5.6 Hz, 1H), 3.30 (dd, J = 18.0, 9.4 Hz, 1H), 2.71 (dd, J = 18.0, 5.6 Hz, 1H).

3-(7-Chloronaphthalen-1-yl)pyrrolidine-2,5-dione (**26**)

Prepared according to the procedure described for compound **25**

LC-MS for $C_{14}H_{10}ClNO_2$+H^+ $[M+H]^+$: calcd. 260.0; found: 260.0. ^{1}H NMR (300 MHz, MeOH-d4) δ [ppm]: 8.08 (s, 1H), 7.95 (d, *J* = 8.7 Hz, 1H), 7.88 (d, *J* = 8.4 Hz, 1H), 7.59 – 7.53 (m, 3H), 4.94 (dd, *J* = 9.6, 5.4 Hz, 1H), 3.44 (dd, *J* = 18.3, 9.6 Hz, 1H), 2.75(dd, *J* = 18.3, 5.4 Hz, 1H).

3-(6-Chloronaphthalen-1-yl)pyrrolidine-2,5-dione (**27**)

Prepared according to the procedure described for compound **25**

LC-MS for $C_{14}H_{10}ClNO_2$-H^- $[M-H]^-$: calcd. 258.0; found: 257.9. ^{1}H NMR (400 MHz, MeOH-d4) δ [ppm]: 8.02 (d, *J* = 9.0 Hz, 1H), 7.96 (d, *J* = 1.8 Hz, 1H), 7.81 (d, *J* = 8.3 Hz, 1H), 7.57 – 7.49 (m, 2H), 7.42 (d, *J* = 7.3 Hz, 1H), 4.96 (dd, *J* = 9.8, 5.3 Hz, 1H), 3.44 (dd, *J* = 18.3, 9.8 Hz, 1H), 2.77 (dd, *J* = 18.2, 5.3 Hz, 1H).

Assay for hIDO-1 enzymatic activity determination: PDMAB assay

To measure enzymatic activity of human hIDO-1, the reaction mixture contained (final concentrations) potassium phosphate buffer (50 mM, pH 6.5), ascorbic acid (10 mM), methylene blue (5 μM) and human recombinant hIDO-1 enzyme (final concentration 5 μg/mL) without or with the test compounds at 10 different concentrations (total volume 112.5 μL). The reaction was initiated by the addition of 37.5 μL of L-Trp (final concentration 100 μM) at room temperature. The reaction was conducted at room temperature during 15 minutes and stopped by the addition of 30 μL of 30% (w/v) trichloroacetic acid. To convert N-formylkynurenine into kynurenine, the reaction mixture was incubated at 65 °C for 30 min. Then 120 μL of 2.5% (w/v) 4-

(dimethylamino)-benzaldehyde in acetic acid were added and the mixture incubated for 5 min at room temperature. Kynurenine concentrations were determined by measuring the absorbance at 480 nm. A standard curve was made with pure kynurenine. The hIDO-1 activity was measured as described above using ten serial concentrations of the compounds to be tested.

Assay for hIDO-1, hIDO-2 and hTDO-2 enzymatic activity determination: LCMS assay

The inhibition of human, dog and mouse IDO-1, human IDO2 and human TDO was measured by quantitating tryptophan and kynurenine by mass spectrometry (MS). hIDO-1 catalyzes the conversion of tryptophan to N-formyl kynurenine. This assay measures the generation of kynurenine by MS which forms quantitatively following non-enzymatic transformation of N-formyl kynurenine. Enzyme (final concentration 1.5 nM hIDO-1, 20 nM TDO, 250 nM hIDO2) was incubated with various concentrations of the inhibitor, in duplicate, at room temperature in assay buffer (Mg^{2+}, Ca^{2+}-free phosphate buffered saline (PBS), 20 mM ascorbic acid, 10 μM methylene blue, 800 nM catalase, 15 μM tryptophan) in a final volume of 100 μL. After 22 minutes, 15 μL of 25% HCl was added to each well. The HCl stops the enzyme reactions and also converts the N-formyl kynurenine to kynurenine. Complete conversion occurs in less than 15 minutes at room temperature. Sealed plates were then transferred to a RapidFire 365 high throughput solid phase extraction (SPE) chromatography system coupled to a 6495 triple quadrupole mass spectrometer (Agilent Technologies, Santa Clara, CA). Detection of tryptophan and kynurenine was accomplished following injection of assay reaction (injection loop volume is 10 μL) onto an Agilent Graphite Type D cartridge in 0.01% trifluoroacetic acid (TFA) plus 0.09% formic acid and eluted using 80% acetonitrile, 0.09% formic acid and 0.01% TFA. The finalized RapidFire settings were as follows: aspiration time: 600 ms or until the loop is full per the sip

sensor, load time: 5000 ms, elution time: 5000 ms, and re-equilibration time: 500 ms at a flow rate of 1.5 mL/min.

Following RapidFire SPE, samples were eluted into an Agilent 6495 triple quadrupole mass spectrometer with an Agilent Jet Stream source with ion funnel technology, set in positive ion mode. A multiple reaction monitoring (MRM) protocol was optimized employing Q1 m/z ratios of 205 and 209 for tryptophan and kynurenine, respectively. The second quadrupole (Q2) was used as a collision chamber employing house nitrogen as the collision gas. The third quadrupole (Q3) was set to select the product ions of tryptophan (m/z = 188) and kynurenine (m/z = 146). Fragmentor voltage was 380 V, collision energy (CE) was 10 V and cell accelerator voltage was 10 V. AUC for tryptophan and kynurenine was quantitated using RapidFire Integrator software version 4.0.13141.13143 (Agilent). For conversion of AUC to pmoles of analyte, standard curves were generated over a range of concentrations from 1 nM up to 1 μM.

IC_{50} values were determined from an 11-point dose response curve by plotting the AUC for kynurenine as a function of inhibitor concentration and fitting the data to the standard four parameter (log [Inhibitor] vs response) equation for enzyme inhibition, using a Pfizer proprietary software package. Each compound was tested a minimum of three times against each species of purified IDO-1 enzyme except for the dog enzyme where there were two replicates. Similarly, there were two replicates for hIDO2 and hTDO. Values displayed are the geometric means of all determinations.

HeLa cellular hIDO-1 assay

To test the hIDO-1 activity in a cellular context, two hIDO1 inducible cell models were used. HeLa cervical carcinoma cells were used as a representative human cancer cell line. HeLa cells were harvested from cell culture flasks using 0.25% Trypsin/EDTA (Gibco-Life Technologies) and neutralized with EMEM growth medium. Following resuspension in fresh growth media, cells were seeded at 20,000 cells per well in 200 µL growth media in a 96-well plate and allowed to adhere at 37°C at 5% CO_2 overnight. The following day, growth media was aspirated and replaced with 200 µL reduced (2%) serum media containing 100 ng/mL recombinant human interferon gamma (rhIFNγ) and incubated at 37°C with 5% CO_2 for 48 hours to induce IDO-1 expression. On day four, compounds were diluted to 10 mM in DMSO and 11-point 3-fold dilutions were prepared. rhIFNγ-containing media was removed and following dilution into EMEM, compounds were added to cells at 50 µM top concentration and allowed to incubate 16-24 hours at 37°C with 5% CO_2. On day five of the assay, 100 µL cell supernatant was transferred to a v-bottom 96 well plate. 30 µL 30% trichloroacetic acid (TCA) was added to each well to precipitate proteins and plates were centrifuged at 3000 RPM for 10 minutes. 100 µL was transferred to a fresh flat-bottom 96-well plate and 100 µL/well 2% 4-(dimethylamino)benzaldehyde (pDMAB) in acetic acid was added to derivatize N-formyl kynurenine to kynurenine for quantitative colorimetric readout. Assay plates were read at A492 on Envision plate reader (Perkin Elmer). IC50 values were calculated using Activity Base software and non-linear regression of percent inhibition versus Log_{10} concentration of hIDO-1 inhibitor compound.

THP-1 cellular hIDO-1 assay

To complement the HeLa cellular assay, an additional assay tested the activity of hIDO1 in the human peripheral blood-derived monocytic THP-1 cell line. THP-1 cells were resuspended into

Iscove's Modified Dulbecco's media (IMDM) containing 4% FBS, plus 100 ng/mL lipopolysaccharide (LPS) and 50 ng/mL rhIFNγ to stimulate hIDO1 expression then seeded at 100,000 cells per well in 100 μL in a 96-well plate. hIDO-1 inhibitor compounds were diluted to 10 mM in DMSO and 11-point 3-fold dilutions were prepared in diluted into IMDM medium and added to cells at 50 μM top concentration and allowed to incubate 16-24 hours at 37°C with 5% CO_2. Following TCA protein precipitation, plates were processed, read, and data analyzed as described above in the 'HeLa cellular hIDO-1 assay' section.

Human Whole Blood Assay

Fresh human whole blood was collected in sodium heparin (20 mL) and gently mixed. All sample and agonist addition steps were followed with a mixing step. LPS (Sigma # L-4391) was added to the whole blood to a final concentration of 25 μg/mL. IFNγ (R&D, 285-IF-100) was added next to a final concentration of 100 ng/mL. The stimulated whole blood was transferred immediately to a 96-well U bottom plate, 200 μL per well. **6** was prepared in DMSO from (0.01-100 μM) and aliquotted to individual wells. The final DMSO concentration was 0.5%. **6** spiked whole blood was incubated at 37 ^{0}C overnight. The next day samples were mixed.

A 20 μL aliquot of plasma was precipitated with 80 μL acetonitrile, vortexed vigorously and centrifuged at 3220 x *g* for 15 minutes at 10° C. An aliquot of the supernatant organic solution was diluted in water prior and spiked with stable labeled isotopes of kynurenine and tryptophan as internal standards prior to analysis.

Kynurenine inhibition was determined by dividing the drug treated internal standard adjusted kynurenine counts by the positive control internal standard adjusted value. The no drug treated sample containing DMSO was used as the positive control.

In order to quantify **6a**, a calibration standard curve was prepared in untreated (i.e., no drug) whole blood.

Inhibitor Binding Studies.

Equilibrium binding studies were performed against different ferric and ferrous forms of human hIDO-1 and binding affinity was determined. Titrations of ferric and ferrous forms of human IDO-1(LJEC-1862A1) with inhibitors were performed with either an open cuvette (ferric $+O_2$) or in an argon environment (ferric, depleted O_2 and ferrous) in a closed cuvette with a silicon septum. Typical binding conditions were 50 mM MOPS buffer (pH 7.0), 4.5 μM human IDO-1 (with 100 fold excess dithionite ferrous form only), 100 μM tryptophan (when used) at RT. Microliter volumes of titrant were added with a gas tight syringe. Analysis of the titration results for K_d^{app} values were carried out using GraphPad Prism 6.0.

Protein Purification.

The full length and truncated (12-403 aa) cDNA for human IDO-1 were cloned into pET24(+) based vector with an N-terminal cleavable his tag. Protein was overexpressed in bacterial cells (BL21(DE3)) with IPTG and purified using Ni affinity column in lysis buffer containing 25mM Tris Cl, pH7.4, 300mM NaCl, 5%Glycerol, and 1mM TCEP plus protease inhibitor cocktails. The non-tagged protein was obtained by TEV treatment of nickel purified protein overnight at 4°C. To

obtain pure and hemin fully loaded protein, 10x molar ratio of hemin dissolved in 25mM NaOH was added slowly to protein and incubated at 4oC overnight followed by anion exchange column with a starting buffer containing 25mM Tris Cl, pH8.0, 25mM NaCl, 5% Glycerol, and 1mM TCEP. The flow through from anion exchange column was concentrated and further purified by size exclusion chromatograph in a buffer containing 25mM Tris Cl, pH8, 150mM NaCl, 5% Glycerol, and1mM TCEP. The full length protein (LJEC-1862A1) was concentrated to 2.6mg/ml for biochemical assays and the truncated protein (LJEC-1863) was concentrated to 24mg/ml for crystallization.

Crystallization, structure determination and refinement

IDO-1 – **6a** complex was prepared by mixing hIDO-1 (LJEC--1863) at 24 mg/ml with 100 mM **6a** in DMSO for a final molar ratio of 4:1 (**6a**: hIDO-1). The mixture was incubated for 1 hr on ice, then centrifuged at 16,100g at 4^{o}C for 10 minutes to remove any insoluble material. Using a Mosquito liquid handler (TTP Labtech), the complex was screened in sitting drop 200 nl + 200 nl drops. Good quality crystals grew in Hampton Research Peg/Ion screen condition #4 (20% PEG3350, 0.2M Lithium Chloride) at 13^{o}C. Crystals were cryopreserved by a 2 minute soak in cryo-solution composed of 14% PEG3350, 140 mM ammonium formate, 21% glucose and 1 mM **6a** before flash cooling in liquid nitrogen.

Diffraction data were collected at 98K at the IMCA-CAT beamline 17-ID at the Advanced Photon Source using a Dectris Pilatus 6M Pixel Array. Data were processed using autoPROC and programs from the CCP4 suite and the structure was determined by molecular replacement using MOLREP using the 2D0T pdb hIDO-1 structure as the search model. Refinement was carried out using autoBUSTER, with cycles of rebuilding in COOT. The statistics of the data processing and

structure refinement are listed in Supplementary Table S1 . Further details of structure refinement are given in the PDB header.

All procedures performed on these animals were in accordance with regulations and established guidelines and were reviewed and approved by Pfizer Institutional Animal Care and Use Committee.

Supporting Information. Full list of compounds not showing significant activity on hIDO-1. Statistics for the crystallographic analysis. Molecular Formula strings. This material is available free of charge via the internet at http://pubs.acs.org. Authors will release the atomic coordinates and experimental data upon article publication.

Accession Codes. Authors will release the atomic coordinates and experimental data upon article publication (**6a**, PDB code: 5WHR).

Corresponding Authors

* To whom correspondence should be addressed. Phone: +3271919932. Fax: +3271919959. E-mail: stefano.crosignani@iteostherapeutics.com. Phone: 858-622-7529. E-mail: martin.wythes@pfizer.com.

Present Addresses

†If an author's address is different than the one given in the affiliation line, this information may be included here.

Author Contributions

The manuscript was written through contributions of all authors. All authors have given approval to the final version of the manuscript. ‡These authors contributed equally. (match statement to author names with a symbol)

Funding Sources

iTeos is supported by the Walloon Region of Belgium and the FEDER (European Fund for Economic and Regional Development).

Conflict of Interest Disclosure

Patrick Bingham, Deepak Dalvie, Jun Li Feng, Samantha Greasley, Stephen E Kaiser, Manfred Kraus, Karen Maegley, Nichol Miller, Brion W Murray, James Soloweij, Al Stewart, Joseph Tumang, Vince Torti, Martin Wythes are current employees or former employees and/or have ownership interest (including patents) in Pfizer.

Stefano Crosignani, Pauline Bottemanne, Hélène Cannelle, Sandra Cauwenberghs, Marie Cordonnier, Frederik Deroose, Bruno Gomes, Manfred Schneider , Benoit Van Den Eynde are current or former employees and/or consultants and may have a business and/or financial interest in iTeos.

ACKNOWLEDGMENT

We are grateful to Jenny Chaplin, Martin Edwards, Stephanie Scales, Theodore Johnson and Jay Srirangam for helpful discussions during the course of this work.

Abbreviations: ABT, aminobenzotriazole; AcOH, acetic acid; ADME, absorption-distribution-metabolism-excretion; AhR, aryl hydrocarbon receptor; ANOVA, analysis of variance; AUC, area under the curve; BID, bis in die (twice a day); BSA, bovine serum albumin; CHO, chinase hamster ovary; Cl, clearance; Clint, intrinsic clearance; CNS, central nervous system; Fu, fraction unbound; Fz, absolute oral bioavailability; HBA, hydrogen bond acceptor; HBD, hydrogen bond donor; hERG, human Ether-à-go-go-Related Gene; IDO-1, indoleamine-2,3-dioxygenase 1; IDO-2, indoleamine-2,3-dioxygenase 2; INFγ, interferon gamma; LCMSMS, Liquid chromatography –

tandem mass spectrometry; LE, Ligand Efficiency; MDR, multi-drug resistance; NADPH, Nicotinamide adenine dinucleotide phosphate; NMP, N-methylpyrrolidinone; p.o., per os (by oral administration); LPS, lipopolysaccharide; MDCK, Madin-Darby canine kidney cells; Papp, apparent permeability; PBS, phosphate buffered saline; PDMAB, *para*-dimethylaminobenzaldehyde; PK, pharmacokinetic; Q_H, liver blood flow; RRCK, Ralph-Russ canine kidney cells; SAR, structure-activity relationship; $t_{1/2}$, half-life; TDO-2, tryptophan-2,3-dioxygenase 2; Vss, volume of distribution at steady state; WBA, whole-blood assay.

References

1. Mahoney, K.M.; Rennert, P.D.; Freeman, G.J. Combination cancer immunotherapy and new immunomodulatory targets. *Nat. Rev. Drug Discovery* **2015**, *14*, 561-584.

2. Munn, D.H.; Mellor, A.L. Indoleamine 2,3 dioxygenase and metabolic control of immune responses. *Trends Immunol*. **2013** *34*, 137–143.

3. van Baren, N.; Van den Eynde, B.J. Tryptophan-degrading enzymes in tumoral immune resistance. *Front. Immunol.* **2015**, *6*, 1-9.

4. Uyttenhove, C.; Pilotte, L.; Théate, I. ; Stroobant, V.; Colau, D.; Parmentier, N.; Boon, T.; Van Den Eynde B.J. Evidence for a tumoral immune resistance mechanism based on typrotophan degradation by indoleamine-2,3-dioxygenase. *Nat. Med.* **2003**, *10*, 1269-1274.

5. Okamoto, A.; Nikaido, T.; Ochiai, K.; Takakura, S.; Saito, M.; Aoki, Y.; Ishii, N.; Yanaihara, N.; Yamada, K.; Takikawa, O.; Kawaguchi, R.; Isonishi, S.; Tanaka, T;. Urashima, M. Indoleamine 2,3-dioxygenase serves as a marker of poor prognosis in gene expression profiles of serous ovarian cancer cells. *Clin. Cancer Res.* **2005**, *11*, 6030-6039.

6. Brandacher, G.; Perathoner, A.; Ladurner, R.; Schneeberger, S.; Obrist, P.; Winkler, C.; Werner, E.R.; Werner-Felmayer, G.; Weiss, H.G.; Gobel, G.; Margreiter, R.; Konigsrainer, A.; Fuchs, D.; Amberger, A. PrognosticValue of Indoleamine 2,3-Dioxygenase Expression in Colorectal Cancer: Effect on Tumor-Infiltrating T Cells. *Clin. Cancer Res.* **2006**, *12*, 1144-1151.

7. Holmgaard, R.B.; Zamarin, D.; Munn, D.H.; Wolchok, J.D.; Allison J.P. Indoleamine 2,3-dioxygenase is a critical resistance mechanism in antitumor T cell immunotherapy targeting CTLA-4. *J. Exp. Med.* **2013**, *210*, 1389-402.

8. Platten, M.; von Knebel Doeberitz, N.; Oezen, I.; Wick, W.; Ochs, K. Cancer immunotherapy by targeting IDO-1/TDO and their downstream effectors. *Front. Immunol.* **2015**, *5*, 673.

9. Röhrig, U.F.; Majjigapu, S.R.; Vogel, P.; Zoete, V.; Michielin, O. Challenges in the discovery of indoleamine 2,3-dioxygenase 1 (IDO1) inhibitors. *J. Med. Chem.* **2015**, *58*, 9421−9437.

10. Beatty, G.L.; O'Dwyer, P.J.; Clark, J.; Shi, J.G.; Bowman, K.J.; Scherle, P.A.; Newton, R.C.; Schaub, R.; Maleski, J.; Leopold, L.; Gajewski, T.F. First-in-human phase I study of the oral inhibitor of indoleamine 2,3-dioxygenase-1 Epacadostat (INCB024360) in patients with advanced solid malignancies. *Clin. Cancer Res.* **2017**, *23*, 3269-3276.

11. Yue, E.W.; Douty, B.; Wayland, B.; Bower, M.; Liu, X.; Leffet, L.; Wang, Q.; Bowman, K.J.; Hansbury, M.J.; Liu, C.; Wei, M.; Li, Y.; Wynn, R.; Burn, T.C.; Koblish, H.K.; Fridman, J.S.; Metcalf, B.; Scherle, P.A. and Combs, A.P. Discovery of potent competitive inhibitors of Indoleamine 2,3-Dioxygenase with in vivo pharmacodynamic activity and efficacy in a mouse melanoma model. *J. Med. Chem*. **2009**, *52*, 7364–7367.

12. Kumar, S.; Jaller, D.; Patel, B.; LaLonde, J.M.; DuHadaway, J.B.; Malachowski, W.P.; Prendergast, G.C.; Muller A.J. Structure based development of phenylimidazole-derived inhibitors of indoleamine 2,3-dioxygenase. *J. Med. Chem.* **2008**, *51*, 4968–4977.

13. Cady, S.G.; Sono, M. 1-Methyl-DL-tryptophan, beta-(3- benzofuranyl)-DL-alanine (the oxygen analog of tryptophan), and beta-[3-benzo(b)thienyl]-DL-alanine (the sulfur analog of tryptophan) are competitive inhibitors for indoleamine 2,3-dioxygenase. *Arch. Biochem. Biophys.* **1991**, *291*, 326−333.

14. Peterson, A.C.; Migawa, M.T.; Martin, M.J.; Hamaker, L.K.; Czerwinski, K.M.; Zhang, W.; Arend, R.A.; Fisette, P.L.; Okazi, Y.; Will, J.A.; Brown, R.R.; Cook, J.M. Evaluation of functionalized tryptophan derivatives and related compounds as competitive inhibitors of indoleamine 2,3-dioxygenase. *Med. Chem. Res.* **1994**, *3*, 531−544.

15. Saito, K.; Chen, C.Y.; Masana, M.; Crowley, J.S.; Markey, S.P.; Heyes, M.P. 4-Chloro-3-hydroxyanthranilate, 6-chlorotryptophan and norharmane attenuate quinolinic acid formation by interferongamma-stimulated monocytes (THP-1 cells). *Biochem. J.* **1993**, *291*, 11−14.

16. Gaspari, P.; Banerjee, T.; Malachowski, W. P.; Muller, A. J.; Prendergast, G. C.; DuHadaway, J.; Bennett, S.; Donovan, A. M. Structure-activity study of brassinin derivatives as indoleamine 2,3- dioxygenase inhibitors. *J. Med. Chem.* **2006**, *49*, 684−692

17. Nakashima, H.; Uto, Y.; Nakata, E.; Nagasawa, H.; Ikkyu, K.; Hiraoka, N.; Nakashima, K.; Sasaki, Y.; Sugimoto, H.; Shiro, Y.; Hashimoto, T.; Okamoto, Y.; Asakawa, Y.; Hori, H. Synthesis and biological activity of 1-methyl-tryptophan-tirapazamine hybrids as hypoxia-

targeting indoleamine 2,3-dioxygenase inhibitors. *Bioorg. Med. Chem.* **2008**, *16*, 8661−8669.

18. Dolusič, E.; Larrieu, P.; Blanc, S.; Sapunaric, F.; Pouyez, J.;́ Moineaux, L.; Colette, D.; Stroobant, V.; Pilotte, L.; Colau, D.; Ferain, T.; Fraser, G.; Galleni, M.; Frere, J.-M.; Masereel, B.; Van den Eynde,̀ B.; Wouters, J.; Fredérick, R. Discovery and preliminary SARs of keto-́ indoles as novel indoleamine 2,3-dioxygenase (IDO) inhibitors. *Eur. J. Med. Chem.* **2011**, *46*, 3058−3065.

19. Dolusič, E.; Larrieu, P.; Blanc, S.; Sapunaric, F.; Norberg, B.;́ Moineaux, L.; Colette, D.; Stroobant, V.; Pilotte, L.; Colau, D.; Ferain, T.; Fraser, G.; Galleni, M.; Galeni, M.; Frere, J.-M.; Masereel, B.; Vaǹ den Eynde, B.; Wouters, J.; Fredérick, R. Indol-2-yl ethanones as noveĺ indoleamine 2,3-dioxygenase (IDO) inhibitors. *Bioorg. Med. Chem.* **2011**, *19*, 1550−1561.

20. Tanaka, M.; Li, X.; Hikawa, H.; Suzuki, T.; Tsutsumi, K.; Sato, M.; Takikawa, O.; Suzuki, H.; Yokoyama, Y. Synthesis and biological evaluation of novel tryptoline derivatives as indoleamine 2,3- dioxygenase (IDO) inhibitors. *Bioorg. Med. Chem.* **2013**, *21*, 1159− 1165.

21. Cavalheiro Tourino, M.; de Oliveira, E. M.; Belle, L. P.;́ Knebel, F. H.; Albuquerque, R. C.; Dörr, F. A.; Okada, S. S.; Migliorini, S.; Soares, I. S.; Campa, A. Tryptamine and dimethyltryptamine inhibit indoleamine 2,3 dioxygenase and increase the tumor-reactive effect of peripheral blood mononuclear cells. *Cell Biochem. Funct.* **2013**, *31*, 361−364.

22. Soret, J.-L. Analyse Spectrale – Sur le spectre d'absorption du sang dans la partie violette et ultra-violette. *C. R. Hebd. Séances Acad. Sci.* **1883**, *97*, 1269-70.

23. Sono, M.; Cady, S.G. Enzyme kinetic and spectroscopic studies of inhibitor and effector interactions with indoleamine 2,3-dioxygenase. 1. Norharman and 4-phenylimidazole binding to the enzyme as inhibitors and heme ligands. *Biochem*istry **1989**, *28*, 5392–5399.

24. Lu, C.; Lin, Y.; Yeh, S.R. Biochem. Spectroscopic studies of ligand and substrate binding to human indoleamine 2,3-dioxygenase. *Biochemistry* **2010**, *49*, 5028-34.

25. Gomes, B.; Driessens, G.; Bartlett, D.; Cauwenberghs, S.; Crosignani, S.; Dalvie, D.; Denies, S.; Fantin, V.R.; Guo, J.; Letellier, M.-C.; Li, W.; Maegley, K.; Marillier, R.; Miller, N.; Pirson, R.; Rabolli, V.; Ray, C.; Streiner, N.; Torti, V.R.; Tsaparikos, K.; van den Eynde, B.; Wythes, M.; Zheng, X.; Tumang, J.; Kraus, M. *Unpublished results.*

26. Crosignani, S.; Cauwenberghs, S.; Driessens, G.; Deroose, F. Pyrrolidine-2,5-dione derivatives, pharmaceutical compositions and methods for use as indoleamine 2,3-dioxygenase-1 inhibitors. PCT Patent WO 2015173764, Nov 19, 2015.

Table of content graphic